2-1-2016

Evaluation of nitrous acid sources and sinks in urban outflow

Elliott T. Gall
Rice University

Robert J. Griffin
Rice University

Allison L. Steiner
University of Michigan

Jack E. Dibb
University of New Hampshire, Durham, jack.dibb@unh.edu

Eric M. Scheuer
University of New Hampshire, Durham, Eric.Scheuer@unh.edu

See next page for additional authors

Comments

This is an Accepted Manuscript of an article published by Elsevier in Atmospheric Environment in 2016, available online: https://dx.doi.org/10.1016/j.atmosenv.2015.12.044.

Recommended Citation

Gall, E. T., R. J. Griffin, A. L. Steiner, J. Dibb, E. Scheuer, L. Gong, A. P. Rutter, B. K. Cevik, S. Kim, B. Lefer, J. Flynn, and R. J. Griffin (2016), Evaluation of nitrous acid sources and sinks in urban outflow, Atmospheric Environment, 127, 272-282, https://dx.doi.org/10.1016/j.atmosenv.2015.12.044

Elsevier Editorial System(tm) for Atmospheric Environment

Manuscript Draft

Manuscript Number: ATMENV-D-15-00799R2

Title: Evaluation of nitrous acid sources and sinks in urban outflow

Article Type: Research Paper

Keywords: urban air quality; nitrous acid; Monte Carlo simulation; evolutionary solver

Corresponding Author: Dr. R.J. Griffin, United States

Corresponding Author's Institution: Rice University

First Author: Elliott T Gall, PhD

Order of Authors: Elliott T Gall, PhD; R.J. Griffin, United States; Allison L Steiner, PhD; Jack Dibb; Eric Scheuer; Longwen Gong; Andrew Rutter; Basak Karakurt Cevik; Saewung Kim; Barry Lefer; James Flynn

Abstract: Intensive air quality measurements made from June 22-25, 2011 in the outflow of the Dallas-Fort Worth (DFW) metropolitan area are used to evaluate nitrous acid (HONO) sources and sinks. A two-layer box model was developed to assess the ability of established and recently identified HONO sources and sinks to reproduce observations of HONO mixing ratios. A baseline model scenario includes sources and sinks established in the literature and is compared to scenarios including three recently identified sources: volatile organic compound-mediated conversion of nitric acid to HONO (S1), biotic emission from the ground (S2), and re-emission from a surface nitrite reservoir (S3). For all mechanisms, ranges of parametric values span lower- and upper-limit values. Model outcomes for 'likely' estimates of sources and sinks generally show under-prediction of HONO observations, implying the need to evaluate additional sources and variability in estimates of parameterizations, particularly during daylight hours. Monte Carlo simulation is applied to model scenarios constructed with sources S1-S3 added independently and in combination, generally showing improved model outcomes. Adding sources S2 and S3 (scenario S2/S3) appears to best replicate observed HONO, as determined by the model coefficient of determination and residual sum of squared errors ($r^2 = 0.55 \pm 0.03$, SSE = $4.6\times10^6 \pm 7.6\times10^5$ ppt^2). In scenario S2/S3, source S2 is shown to account for 25%and 6.7% of the nighttime and daytime budget, respectively, while source S3 accounts for 19% and 11% of the nighttime and daytime budget, respectively. However, despite improved model fit, there remains significant underestimation of daytime HONO; on average, a 0.15 ppt/s unknown daytime HONO source, or 67% of the total daytime source, is needed to bring scenario S2/S3 into agreement with observation. Estimates of 'best fit' parameterizations across lower to upper-limit values results in a moderate reduction of the unknown daytime source, from 0.15 to 0.10 ppt/s.

Department of Civil and Environmental Engineering
George R. Brown School of Engineering

December 14, 2015

Managing Editor
Atmospheric Environment

To Whom It May Concern:

Enclosed please find a revised manuscript entitled 'Evaluation of nitrous acid sources and sinks in urban outflow' by Elliott Gall (currently at the Nanyang Technological University & Berkeley Education Alliance for Research in Singapore, 1 Create Way #11-01 Create Tower, Singapore 138602) et al. This manuscript has not been published previously (in whole or in part) nor is it currently under consideration for publication in any other journal. All authors know and approve of its submission.

This manuscript provides an updated description of a combination of measurements and modeling to elucidate the dynamics of nitrous acid (HONO) in the outflow of the Dallas-Fort Worth (DFW) metropolitan area. In this work, we extensively review the literature and develop a two-layer model that incorporates various HONO source and sink mechanisms promulgated in the literature. Of these, three are recently identified (2013-2014). For all, a range of values spanning a 'lower-limit', 'likely', and 'upper-limit' is defined. The three recently identified mechanisms are integrated into the model first through a full-factorial screening analysis to observe their potential to resolve disagreement between modeled and measured HONO mixing ratios. Promising scenarios are further evaluated in two ways: with an evolutionary solver and Monte Carlo simulation. These approaches allow the range of possible values for each mechanism to be input stochastically and create a quantitative estimation of the likelihood of a combination of source and sink mechanisms to replicate observed HONO mixing ratios. Given the incomplete understanding of HONO dynamics in the troposphere, and the many proposed mechanisms in the literature to account for "missing HONO", we believe this investigation improves the state of understanding of HONO dynamics. More broadly, the approach developed here (deterministic screening analysis, evolutionary solver to compare "best-case" parameters for scenarios, followed by in-depth Monte Carlo simulation) is a logical approach that may be used to evaluate potential sources and sinks of other atmospheric constituents. Our response to this second round of reviews is included in a separate document. The SI has been updated accordingly. I also wish to acknowledge the thorough, thoughtful, and helpful reviews that have improved our manuscript.

I look forward to your favorable response. Please let me know if I can be of any assistance.

Sincerely,

Robert J. Griffin, Ph.D.

Rice University · Department of Civil and Environmental Engineering – MS 318 · George R. Brown School of Engineering
6100 Main Street · Houston, Texas 77005 · Phone: (713) 348-2093 · Fax: (713) 348-5268 · E-mail: rob.griffin@rice.edu

Reviewer #3: General comments:

In revised manuscript by Gall et al. a two layer model was developed to describe sources and sinks of nitrous acid (HONO) and results were compared to ambient field measurements. Different sources recently postulated were added to a base case model and parameters were optimized to best describe the experimental observations.
The revised manuscript was significantly improved and I recommend publication after a few concerns have been considered

Response:

We thank reviewer 3 for the additional detailed review. We believe the corrections, recommendations, and feedback have further improved the manuscript.

Note that line numbers referring to the SI are called out as Lines SI: XX-XX whereas line numbers referring to the main manuscript are called out as Lines XX-XX.

Major concern:
I still have some concerns with the parameterization of the used sources:

Response:

Parameterizations will be updated according to the suggestions made. See below for specific responses to each comment/recommendation.

B1 (NO2 conversion on aerosols, Supplement page 2):
For the surface to volume ratio used (A), the surface of the soot should be subtracted. The soot surface is already used for source B3 and cannot react double.

Response:

For Source B3, soot particles were measured with an aethelometer that reported in units of $\mu g/m^3$, while for sources B1 and B2, a SEMS reported the size-resolved number concentration. As we do not have size distribution data for soot particles, we have reduced the number size distribution available for Sources B1 and B2 by an approximation of the surface area of soot particles. The surface area of soot particles was estimated to first approximation by assuming the ratio of the mass contribution of BC to that of the total particle mass loading is the same as the surface area contribution of BC to that of the total particle surface area. This assumption reduced the available surface area for mechanism B1 by an average of 6% across the model period.

This change has been implemented to the model and described in the supporting information in Lines SI: 41-48 which read:

The estimate of $(SA_{meas})i$, was reduced to account for black carbon (BC), as BC particles are taken to react as described in mechanism B3 and are assumed not available for reaction as described in equation S1. As the aethelometer used in this investigation did not provide size-resolved data, values of $(SA_{meas})i$ were reduced by the ratio of the mass of BC particles determined with the aethelometer to the total particle mass determined with an aerosol mass spectrometer (AMS). On average, this resulted in the reduction of total particle surface area of 6% from values measured with the SEMS.

B2 (Photoenhanced uptake of NO2 on aerosols, Supplement page 3):
The used uptake kinetics is extremely fast, which has to my knowledge not yet been observed for any realistic surfaces in lab studies. The reference to Wong et al. does not help here, since also there no reference is specified. Since a yield of 1 is considered the reactant should be oxidized by NO2 (e.g. OC). However, typical uptake coefficients vary only between 10^-6 and few times 10^-5 for organic surfaces (aromatic VOCs, humic acids, see e.g. Stemmler et al., 2007). The 2NO2+H2O reaction is even slower, not photoenhanced and has only a max. yield of 0.5. There is one exception, which is the photocatalytic conversion of NO2 on pure TiO2 aerosols, which can reach uptake coefficients >10^-4 (see Gustafsson et al., 2006). However, HONO yields can only reach 0.5 and it is not expected that the TiO2 content in atmospheric particles is higher than a few % at maximum (=> lower average gamma). Here further references (lab studies…?) are necessary, or the kinetics has to be
defined as speculative, or realistic uptake coefficients (see B8) have to be applied also for source B2.
In addition also here the surface of soot has to be subtracted (see source B3).

Response:

The surface of soot has been subtracted according to the procedure outlined above. We recognize that the kinetics implemented here are faster compared to most experimental determinations made in the literature. As noted by the reviewer, we based the range shown in Table 1 for B2 on modeling work done by others (Wong et al., 2013). We have reduced the 'lower-limit' and 'likely' estimates to be more aligned with the experimental literature, and have left the upper-limit value as previously listed to enable exploration and speculation of faster light-enhanced conversion of aerosol surfaces (similar to as performed by previous modeling studies). In the text, we have added additional description that identifies this upper-limit value as based on previous modeling studies, rather than direct experimental evidence.

Lines SI: 58-66 of the SI now read:

"The un-scaled uptake coefficient shown in Equation S3 was taken from Stemmler et al. (2007) and Wong et al. (2013), ranging from an upper-limit value of 1.0×10^{-3} (used when only aerosol processes were considered in Wong et al. (2013)) to a lower-limit value of 4.0×10^{-6}, in the range of values determined for humic acid aerosols under irradiation with visible light (Stemmler et al. 2007). The 'likely' parameterization is taken from experimental values determined in Stemmler et al. (2007) for RH values similar to those in this investigation. The use of an upper-limit value from Wong et al. (2013) is largely speculative, and enables the evaluation of a stronger photoenhanced aerosol HONO source in the Monte Carlo analysis and evolutionary solver. A HONO yield of 1 was assumed for photoenhanced conversion on aerosols."

We also address this in the main manuscript when presenting the results of the "optimized" model parameterizations at Lines 365-370:

"Aerosol processes increase substantially as a result of a speculative upper-limit as described in the SI; B1 was allowed to vary over an order of magnitude and B2 over 2.5 orders of magnitude based on prior modeling studies, rather than experimental estimates. However, contributions from B1 and B2 remain limited (< 1% as can be determined from absence of B1 and B2 in Figure 4), in part a result of the two layer box-model used here that emphasizes ground-level phenomena."

Times used for B1/B2 (Supplement page 2):
A more simple and correct approach would be a 24 h use of B1 and a use of B2 correlating with J(NO2). It is not expected that the slower 2NO2+H2O dark reaction (B1, yield = 0.5) stops during daytime… In addition, this would avoid any "steps" in the production rates.

Response:

We have updated this mechanism such that B1 is ongoing for 24 hours/day and B2 is correlated with JNO2 as shown in equation S3 of the supporting information. This change is also evident in the revision to equation S4 shown in the Supporting Information

B3 (conversion on soot, supplement page 4):
In the revised manuscript the dark conversion of NO2 was not any more considered and only the photoenhanced conversion on soot was well considered (B3). However, for completeness, I would still add the initial fast conversion in the dark (10^14 HONO cm^-2) scaled with the soot loading and the expected lifetime of soot since emission, see my last report. If the source strength (small) is the argument, also other sources could be neglected…

Response:

The reviewer's point is well-taken that the source should not be removed only due to small source strength. We have made this decision based on not only the source strength being insignificant, but also due to the unknowns that manifest in attempting to implement this parameterization. To account for the fact that soot may only react once with NO_2 to form HONO in the absence of light, an estimate of the injection rate of fresh soot is needed. This estimate cannot be obtained without extensive assumptions that remove the value of undertaking such an exercise for a parameterization that, even in the extreme upper-limit, will not contribute meaningfully to HONO mixing ratios. This is explained more fully in the SI at Lines SI: 89-102 which read:

"Conversion of NO_2 to HONO on soot during the nighttime is thought to occur once per reactive site and therefore soot is likely to rapidly deactivate in the absence of light (Monge et al., 2010). For this reason, an accurate estimate of light-independent conversion on soot requires an estimate of the "injection rate" of fresh soot (Aumont et al. 1999), an estimate we are not able to obtain in this investigation. We justify the exclusion of light-independent conversion on soot by considering an upper-limit scenario where BC mass at each time-step is assumed to be "fresh" and conversion

of NO_2 is instantaneous and not limited by availability of NO_2. The average BC mass concentration is this investigation is 0.35 µg/m^3 over the duration of the model period. With a BET surface area of 122 m^2/g (Monge et al. 2010), f_{soot} of 1×10^{14} molec/cm^2 (Kalberer et al. 1999), and a soot lifetime of 5 days, these upper-limit conditions give an 8-h integrated, light-independent production of HONO of only 0.1 ppt, or an equivalent source strength of 4×10^{-6} ppt/s. Given the uncertainty in implementing this parameterization (i.e., the injection rate of fresh soot is actually unknown), and the insignificant contribution, this source is not considered further in the model here."

B4 (direct emissions, supplement page 5):
As likely HONO/NOx emission ratio (0.0029), the tunnel study of Kirchstetter et al. was used. However, in this study only gasoline vehicles were studied (diesel trucks were not allowed to pass the tunnel). Since diesel vehicles show higher HONO/NOx (and NOx) emissions, a realistic emission ratio for the US should be in between both cited studies, since the diesel faction is lower in the US compared to Germany. This is confirmed by the "best estimates" parameters (0.0044-0.0061, see table 2). .

Response:

We have updated the range of parameterizations in B4 to better reflect the distribution of traffic in the US. The 'lower-limit' value remains as taken from Kirchstetter for a gasoline-only tunnel, while the upper-limit value is now 0.008 as reported in Kurtenbach 2001 for a tunnel of 6% heavy duty trucks, 6% commercial vans, 12.3% diesel and 74.7% gasoline fueled cars. We use an average of the two studies (0.0055) as the 'likely' value. This change is detailed in Lines SI: 105-112 of the Supporting Information:

"where the value of f_{emiss} is ranging from a 'lower-limit' condition of 0.0029 (Kirchstetter et al., 1996) to an 'upper limit' of 0.008 (Kurtenbach et al., 2001). The 'likely' condition is an average of the upper and lower-limit values (0.0055), logical as the value from Kirchstetter et al. (1996) is for a tunnel that allowed only gasoline-powered vehicles while Kurtenbach et . (2001) is for a tunnel in Germany through which a mixture of 6% heavy-duty trucks, 6% commercial vans, 12.3% diesel vehicles, and 74.7% gasoline-fueled cars passed. We expect the typical US to lie in between these studies, given the lower fraction of diesel powered vehicles in the US than in Germany."

B5 (NO+OH, supplement page 5):
In table 1, k(zero) (=3. order kinetics) and k(infinite) (=2. order kinetics) are mixed (typo?). Please check the Troe calculations.

Response:

The values in Table 1 are a typo – we have double-checked the Troe calculations and the correct values were used in calculating the effective second order rate constant (that is, as the reviewer notes k(zero) with units corresponding to 3rd order and k(infinite) corresponding to 2nd order kinetics.

B6 (HNO3-photolysis):
The first term in equation S9 (supplement page 7) is not correct, since the unit would be ppt s^-2… This source should be parameterized with the modelled HNO3 surface concentration (deposition/loss), leading to a HONO surface flux density (molec. cm^-2 s^-1) to be converted into ppt/s in the lower box.

Response:

We have revised the parameterization of B6 to correct the units discrepancy. We have followed the parameterization of Zhou et al. (2003) doi:10.1029/2003GL018620 shown there in Equation 1. The formulation of B6 is now:

$$F_{B6} = a\frac{v_{d,\mathrm{HNO_3}}}{h}\left[\mathrm{HNO_3}\right]j_{\mathrm{HNO_3}}t + \left[\mathrm{pNO_3^-}\right]j_{\mathrm{HNO_3}}\frac{RT}{M\times P}\frac{\frac{1m^3}{1000L}}{\frac{10^6\mu g}{g}}10^{12}$$

where a is the fraction of deposited HNO3 on surfaces exposed to full noontime sunlight with photolysis rate j_{HNO3} (1/s), assumed to be ¼ as in Zhou et al. (2003) and t the accumulation time of HNO_3, taken as the timestep of each calculation. These assumptions imply that the surface HNO3 is exposed to, on a diurnal average, ¼ of the full value of jHNO3, as described by Zhou et al. (2003). This updated equation is included and described in Lines SI: 137-147 of the Supporting

Information.

Parameterization of all ground sources:
Although indeed the transport limitation may not be significant for the very high wind speed during the campaign (high turbulent mixing), the concept shown in equation S12 could be used for all ground processes. Otherwise, when the model is used for more calm conditions (low WS) in the future, transport limitations may get important again. This would avoid any future discussions…

Response:

Uptake of NO_2 at the ground, both light independent and photoenhanced are now parameterized with the R_a and R_b calculated as described in Equations S10-S13 of the Supporting Information.

Definition of "upper" and "lower" limits used is confusing and should be once defined at the beginning. For loss terms (e.g. L1, supplement page 9) high deposition velocities are used as "lower limit", see e.g. line S150. Later I understood that (lower limit = less modelled HONO), but first this was confusing.

Response:

This approach is described in the main manuscript in Lines 212-216. As some readers may refer to the SI before reaching this point in the manuscript, we have added a similar description at Lines SI: 30-34 of the Supporting Information.

S1 (Reduction of HNO3 by VOCs, main page 7):
Although that is partially mentioned at the very end of the document (section 3.6) the used source is highly uncertain, unrealistic and is most probably overestimated. The authors used here production rates, which were determined for a saturated motor oil steam in the lab (Rutter et al.), with an estimated VOC oil concentration of ca. 200 ppb (= several ppmC of a high molecular oil). However these conditions are far away from those during the field campaign for which a daytime (HNO3 only high during daytime…) TOC concentration of only ca. 10 ppb was measured (2-3 orders of magnitude lower…, see figure S8). In addition in Rutter et al., neither the VOC concentration or composition was determined, nor could the authors identify the reactive VOC species (most VOCs do not react with HNO3). Thus, for the smaller VOCs to be expected in the field campaign the majority will be even less reactive against HNO3 compared to motor oil steam. E.g. for propene ("propylene"), I do not know
any lab study which has shown any fast conversion of HNO3 to HONO, and I am quite sure that the reaction will be quite slow (and with NOx as a major product…). But here it is proposed that the HNO3 normalized HONO formation rate at high atmospheric VOC levels (or high propene/benzene ratio…) is similar to the lab study in Rutter et al., see equation (4). In reality the rates will be orders of magnitude lower. If this source should still be considered here (and I would not do as long as reactive species are identified…), I would use at least the total VOC levels in Rutter et al. (ppmCs…) and the present study (5-60 ppbC) for normalization (and even than the source is overestimated caused by the different VOC composition lab/field…).

Response:

The reviewer's concerns regarding the parameterization of source S1 are well-taken. However, the reviewer's recommendations are unclear regarding the suggestion for the additional normalization. Rutter et al. (2014) report an estimated VOC concentration of ~200 ppt rather than 200 ppb (three orders of magnitude lower than the reviewer states, see Table 1 of Rutter et al. 2014 under "estimated oil vapor concentration which ranges from 50-383 ppt). Following the reviewer's logic, this would imply the equivalent of several ppbC, rather than several ppmC of high molecular weight oil and would in turn follow that the laboratory conditions are on the order of magnitude of TOC concentrations we observe in this field investigation (~10 ppb as noted by the reviewer). Furthermore, we re-formulated this parameterization using the propylene/benzene ratio not to directly imply that propylene itself is the reactive VOC of interest, but rather as a proxy for reactive species as propylene is known to be reactive. Benzene, as a longer-lived constituent is present to account for dilution that may occur as air masses travel from downtown DFW to the EML site. This parameterization has an effect of tempering the source strength, in alignment with the reviewer's suggestions –Figure S7 of the Supporting Information shows that the ratio of propylene/benzene at EML to the same ratio at DFW is only elevated during morning rush hour. At all hours other than the 06:00-09:00 timeframe, this ratio results in an ~70-90% reduction of the source strength reported in Rutter et al. 2014. In the 06:00-09:00 time frame, it results in a 20% reduction. As noted by the reviewer, the ratio of HNO_3 at the site to the HNO_3 value used in Rutter provides a further

normalization that reduces the source strength from what is presented in Rutter, on average an ~80% reduction. Therefore, our parameterization seems aligned with the reviewer's assertion that the rates in the field will be lower than that observed in the laboratory (compounding the two normalizations results in, on average, a ~96% reduction compared to the source strengths reported directly by Rutter et al. (2014)). Our findings also seem in agreement with the reviewer, in that, we see a very small contribution from this mechanism and that the inclusion of the mechanism was not observed to improve the model's ability to reproduce observed HONO.

We agree with the reviewer's caution however, and given the speculative nature of this parameterization, we have added the following comments into the main manuscript:

Lines 178-185: Normalizing assumptions shown in equation 4 resulted in, on average, ~95% reduction of fHNO3,VOC when calculating F_{S1}. The form of the parameterization in equation 4 is speculative; propylene is chosen as a proxy for reactive VOCs while benzene is chosen to account for dilution that may occur as air masses move from DFW to EML. Identification of specific reactive species participating in the HONO formation process identified in Rutter et al. (2014) would enable improvements in developing and assessing parameterizations of VOC-mediated conversion of HNO3 to HONO.

S2 (bacterial nitrite production, main page 8):
If there are no typos in tables 1 and 2 (?), this soil ground source is strongly overestimated. For the cited soil surface (grassland and pasture) from Oswald et al. (2013) only optimum HONO fluxes of a few ng N m^-2 s^-1 can be estimated from their figure 2. If this is converted into the units specified in Tables 1 and 2, I get values for F(soil) of ca. 10^14 molec m^2 s^1 = 10^10 molec cm^2 s^-1, which are in fare agreement with direct measured fluxes in the atmosphere (e.g. Ren et al.). However, in table 1 and 2 more than 3 orders of magnitude higher values are specified (and table 1 and 2 are consistent, thus no typo…). Please check the calculations of source S2.
Besides that, the "optimum" fluxes from Oswald et al. were considered here, which were found to be up to 250 ng m^-2 s^-1 in the lab. Since these experiments were performed under unrealistic conditions (the soil is dried by 0% r.h. air => disturbance of biochemistry + low surface adsorption on the drying soil…) and only maximum values are specified (when the soil surface is already dried…), these results do not represent realistic average HONO fluxes by this bacterial nitrite production mechanism. This is inline with direct observed fluxes over natural surfaces of only 0.5-2 ng m^2 s^1.

Response:

In this investigation, we use the direct observed fluxes over natural surfaces that are in the range of 0.4 – 0.9 ng m^-2 s^-1 that are reported in Figure 2 of Oswald et al. In unifying units for presentation in Table 1, there was an error that caused this discrepancy that is not present in the model. We have added the full unit conversion into equations S21-S24 in the supporting information including units conversion for clarity. For example, using the 0.5 ng m^2 s^1 noted by the reviewer:

$$f_{soil} = 0.5\ \frac{ng\ N}{m^2\ s} \times \frac{1\ mol}{14\ g\ N} \times \frac{1\ g\ N}{10^9\ ng\ N} \times 6.0223 \times 10^{23}\ \frac{molecule\ N}{mol\ N} = 2.15 \times 10^{13}\ \frac{molec}{m^2\ s}$$

$$F_{S2} = \frac{f_{soil}}{h} = \frac{2.15 \times 10^{13} \frac{molec}{m^2\ s}}{36\ m}$$

$$F_{S2} = 5.97 \times 10^{11}\ \frac{molec}{m^3\ s} \times \frac{1\ mol}{6.0223 \times 10^{23} molec} \times 0.0821\ \frac{L\ atm}{mol\ K} \times \frac{298\ K}{1\ atm} \times \frac{1\ m^3}{1000\ L} 10^{12}$$

$$F_{S2} = 0.024\ ppt/s$$

As can be determined from Figure 4 of the manuscript, this in near agreement to source strengths associated with S2 from model calculations. The 'likely' scenario reported there shows S2 accounts for 7% of the total daytime source (0.07*0.22 ppt/s = 0.015 ppt/s).

This example calculation is provided in the SI in equations S21-S24 to illustrate the units conversion process undertaken for source S2.

S3 (acid displacement, main page 8):
May be I not understood correctly the parameterization of the source, but how can the HONO reservoir been exhausted until noon (=max. before noon), see line 194. In the recent study by Vandenboer et al., 2015, where this source was also used in a model, there was a realistic maximum of the source flux in the early afternoon (see their Fig. 4c). HNO3 maximize in the afternoon, see Figures 1 and the acid

displacement is proportional with the acid level, see equation (6)? In addition, the nitrite reservoir will be never zero (s. line 193), since HONO is never zero? Here more explanations are necessary.

Response:

We constrained mechanism S3 based on several assumptions that have been given additional clarification in the manuscript and SI. The input to the nitrite reservoir was calculated solely based on the flux of gas-phase HONO to the surface. This results in a surface nitrite reservoir that is limited in quantity such that it can be exhausted based on the displacement from deposition by HCl and HNO_3 present during the 8:00-12:00 local time and early afternoon hours (our site is characterized by relatively high HNO_3 concentrations in the 8:00-12:00 local time morning hours). The statement that the nitrite reservoir is "exhausted" has been be removed for clarity, as it was intended to refer to the first time step during the daytime where displacement by HCl and HNO_3 results in a zero value for the reservoir. During the next time step, because S3 is effectively 0, the reservoir can be replenished due to HONO deposition. Essentially, after the first "exhaustion" of the HONO reservoir, Source S3 alternates between 0 and a positive value, a lag at each time step in the model due to discretization. Vandenboer, 2015 do in fact state that there does not need to be mass-balance closure in any 24-h period and that there may be additional sources supplying the surface nitrite reservoir. For these reasons, we state in main manuscript in Lines 205-209 that we assume this is a conservative estimate of S3.

"As there may be additional sources of surface nitrite other than gas-phase HONO and surface nitrite accumulation over greater than diurnal time-scales, equation 6 likely represents a conservative estimate of the source strength of S3. Further description of the constraints on S3 is given in the SI and dynamics are depicted in Figure S8, also in the SI."

We have also updated the SI with additional description and Figure S8 illustrating the dynamics of constituents associated with S3 at Lines SI: 273-284 of the SI.

Specific comments:
The following comments are listed in the order how they appear in the manuscript.

a) main manuscript:
Line 66: First model studies on this issue may be also mentioned (Staffelbach et al., 1997, or Vogel et al., 2003).

Response:

We have amended this line to include the Staffelbach et al. study.

Line 67, "hypothesized": while some source are indeed speculative, the NO+OH reaction is absolutely certain…

Response:

We have edited the line to separate the confirmed vs. speculative homogeneous sources.

Lines 66-70 now read: "A number of photochemically driven homogeneous reactions have been identified or considered: e.g., the known reaction of OH and NO and the hypothesized reaction of photolytically excited nitrogen dioxide (NO2) and water (Li et al., 2008). The latter, however, may not proceed sufficiently rapidly or at adequate yields to affect HONO mixing ratios in the atmosphere (Carr et al., 2009)"

Line 81: Use only references where this source was directly studied (e.g. George et al., 2005).

Response:

We have reviewed the references and updated according to the reviewer's recommendation (removing Spataro and adding George)

Equation (2): The HONO level by direct emission is overestimated here, since HONO will quickly photolyze during daytime during the time until measured NOx was emitted. But I also not know how to improve that in a box model. Simply mention as uncertainty…

Response:

This limitation is addressed following presentation of equation 2 in Lines 142-143 which read:

Equation 2 may overestimate the contribution of B4 in a box-model, as during the daytime, HONO will rapidly photolyze prior to the measurement of emitted NOx.

Line 227: If NO2 is photolysed it will be not lost, but converted into NO, and for high O3 during daytime, the Leigthon equilibrium will be shifted back to NO2 (see low NO levels in Fig 1). Check if the HONO/NOx ratio also shows a maximum during daytime to confirm the daytime source. In addition the argument with the convective dilution of NO2 does not hold, since HONO is similarly diluted (delete).

Response:

The statement after what is now Line 241 ("… although daytime mixing ratios…. During the day) has been deleted. (note, line was after "…indicative of a secondary daytime source)

Line 234-235: HONO decrease mainly by the convective dilution during daytime (compare NO2 profile and see max. in HONO/NO2 during daytime, strong daytime HONO sources…).

Response:

The results shown in Figure 4 imply that in the first layer of the box model, the major loss is due to photolysis rather than convective transport to the second model layer. Obviously, one limitation of this study is the lack of vertical measurements of HONO (e.g., the presence of a stronger gradient would increase loss due to convective dilution). Therefore, we have edited this line to include both convective dilution and photolysis as dominant loss mechanisms.

Lines 246-248 now read: Mixing ratios of HONO show accumulation over the nighttime and suppression during the daytime, a result of the strong loss due to photolysis and convective dilution during the daytime hours.

Lines 246-248: The underestimation of HONO when vertical transport was considered in the model, results from the fact that here only a two box model was used and that HONO was measured at the lower height (10 m) of the lower box (0-36 m). Caused by the continuous gradient of HONO, the modelled average box concentration is lower. This may be explained here, with the outlook for future real 1D model calculation (finer vertical resolution…). But it is nice that the vertical transport is discussed here!

Response:

We have included a statement at Lines 263-267 regarding the limitation of single HONO measurement in a first-layer box that itself is subject to a vertical gradient.

"The underestimation may also result from the limited vertical resolution in the two-layer box model used here and the measurement height in the lower portion of the first layer (10 m); it is likely that a continuous HONO gradient is present in the 36 m of the model first layer resulting in a lower modeled mixing ratio across the first model layer than the 10 m observation."

Lines 318-321: I cannot understand the contribution of the acid displacement (S3) at night. In line 187 it is mentioned that this source is set to zero at night? In addition, while S2 may be active during daytime, it will be definitely less important during nighttime (less biological activity, higher soil humidity), besides the general issue to that source mentioned above.

Response:

The parameterization for "night" and "day" was set based on the photolysis constant of HONO as a reference for "daytime" in calculations, subject to slight day-to-day variability when non-zero values began and ended. We grouped nighttime from 21:00-07:00 local time to roughly correspond with local sunrise and sunset. There were several instances of non-zero j_{HONO} values that extended beyond 21:00. Due to the relatively low total nighttime HONO source strength, a small contribution from S3 resulted in a few percentage points contribution to the nighttime HONO source. In reformulating this mechanism, we no longer consider S3 as a "daytime" only mechanism,

consistent with Vandenboer et al. (2015), where lower, but non-zero fluxes due to nitrite displacement can be observed in Figure 4c of Vandenboer et al. (2015) in the nighttime hours.

Regarding the limitation for the biological source (S2), we have added the following statement to the conclusions section regarding this potential impact on the source at Lines 428-431.

"Source S2 was parameterized using a single value for a model simulation; there are likely to be diurnal variations in biological activity and soil water content that would impact the parameterization of source S2"

Lines 420-421: better mention the order of all important sources (not only S2/S3…).

Response:

The conclusion has been reworked to include other considered sources in addition to S2 and S3. Lines 451-455 now read:

"Model output for GrN S2/S3 accounted for, on average, 33% of the daytime HONO budget and 103% of the nighttime HONO budget. Major nighttime sources included (in order) NO_2 conversion at the ground (B7), biotic release from soil (S2), and re-emission from the nitrite reservoir (S3). Major daytime sources also include S3, S2, photoenhanced NO_2 conversion at the ground (B8), B8, and the reaction of OH with NO (B5)."

References general:
Use subscript numbers in formula.
Unify stile of the journals names (no abbreviations used in Atmospheric Environment, e.g. line 437: Atmos. Environ.).

Line 434: Pätz, H.-W.
Line 435: …Atmos. 108 (D4), 8247…
Line 444: 336b
Line 447: D20303
Line 484: 1326-e
Line 504-505: Atmos. Chem. Phys., 2011, 11, 10433-10447
Line 510-511, Order of the names: Stemmler, K., M. Ndour, Y. Elshorbany, J. Kleffmann, B. D'Anna, C. George, B. Bohn, M. Ammann,… Atmos. Chem. Phys., 2007, 7, 4237-4248.
Line 518: …Surfaces - a Physical-Chemical…, Dissertation, Universität Heidelberg, 2004, http://www.ub.uni-heidelberg.de/archiv/ 4814.
Line 520: Pszenny, A. A. P.
Line 542: 1326-d
Line 550: 30(23), 2217

Response:

References have been updated according to the reviewer's recommendations.

Tab. 1:
B5: Exchange k(zero) and k(infinite), cf. JPL
S2: should be in (molec m^-2 s^-1), only typo or also used in the model?

Response:

As mentioned above, this is a typo that has been corrected in the presentation of the Table 1.

Tab. 2
B5: Exchange k(zero) and k(infinite), cf. JPL
S2: should be in should be 5.0x10^13 molec m^-2 s^-1, only typo or also used in the model?

Response:
As mentioned above, B5 and S2 have been corrected.

Fig. 4 top, right:
There is no source B1 during daytime, should be B2 which is missing?

Response:

As previously implemented, B1 and B2 were parameterized together with the value of the uptake coefficient used based on time of day, therefore the reviewer is correct in that the daytime aerosol uptake of NO2 should be B2. We have now separated these two processes based on the reviewer's recommendation that B1 will occur in parallel to B2 during the daytime. However, this separation has resulted in <1% contribution from each of these mechanisms, and neither B1 nor B2 are presently included in Figure 4.

b) Supplement:
Equation S1: typically A stands only for the surface and S/V is used for the term mentioned here.

Response:

We have changed the naming of this term to be SA_{meas} consistent with other literature in Atmospheric Environment (e.g. Park et al., 2009 doi:10.1016/j.atmosenv.2008.10.020)

Line 89: If equation (S7) is used both units should be molecular (hopefully ppt is not used here for NO…).

Response:

This typo has been corrected; units for NO are molec/cm^3.

Lines 189-191: For both periods daytime temperatures are lower than during night-time? Typo?

Response:

The daytime and nighttime temperatures were reversed, this typo has been corrected.

Line 207: Kh(z,t) is not shown in Figure 1?

Response:

Kh(z,t) has been added to Figure 1 and the reference in the SI corrected (should have referred to Figure S5).

***Highlights (for review)**

- A two-layer box model evaluates HONO sources, sinks in outflow of Dallas-Fort Worth
- Monte Carlo simulation is applied to scenarios with 3 recently identified sources
- Improved model outcomes result from inclusion of 2 of 3 recently identified sources
- A substantial unknown source is still required for agreement with observation
- Missing HONO source is moderately correlated with j_{NO2}, weakly correlated with NO_2

Evaluation of nitrous acid sources and sinks in urban outflow

Elliott T. Gall[1,2,3], Robert J. Griffin[1*], Allison L. Steiner[4], Jack Dibb[5], Eric Scheuer[5], Longwen Gong[1,6], Andrew P. Rutter[1,7], Basak K. Cevik[1], Saewung Kim[8], Barry Lefer[9,10], James Flynn[9]

[1]Rice University, Department of Civil and Environmental Engineering, Houston, TX 77005
[2]Portland State University, Department of Mechanical and Materials Engineering, Portland, OR 97201
[3](Current) Nanyang Technological University & Berkeley Education Alliance for Research in Singapore, Singapore 138602
[4]University of Michigan, Department of Atmospheric, Ocean, and Space Sciences, Ann Arbor, MI 48109
[5]University of New Hampshire, Earth Systems Research Center, Durham, NH 03824
[6](Current) California Air Resources Board, Monitoring and Laboratory Division, Sacramento, CA 95811
[7] S.C. Johnson, Inc., Collaborative Sciences Division, Racine, WI 53403
[8]University of California – Irvine, Department of Earth System Science, Irvine, CA 92697
[9]University of Houston, Department of Earth and Atmospheric Sciences, Houston, TX 77004
[10] NASA Headquarters, Tropospheric Composition Program, Washington, DC 20546

[*]Corresponding author: Robert J. Griffin (rob.griffin@rice.edu)

ABSTRACT

Intensive air quality measurements made from June 22-25, 2011 in the outflow of the Dallas-Fort Worth (DFW) metropolitan area are used to evaluate nitrous acid (HONO) sources and sinks. A two-layer box model was developed to assess the ability of established and recently identified HONO sources and sinks to reproduce observations of HONO mixing ratios. A baseline model scenario includes sources and sinks established in the literature and is compared to scenarios including three recently identified sources: volatile organic compound-mediated conversion of nitric acid to HONO (S1), biotic emission from the ground (S2), and re-emission from a surface nitrite reservoir (S3). For all mechanisms, ranges of parametric values span lower- and upper-limit values. Model outcomes for 'likely' estimates of sources and sinks generally show under-prediction of HONO observations, implying the need to evaluate additional sources and variability in estimates of parameterizations, particularly during daylight hours. Monte Carlo simulation is applied to model scenarios constructed with sources S1-S3 added independently and in combination, generally showing improved model outcomes. Adding sources S2 and S3 (scenario S2/S3) appears to best replicate observed HONO, as determined by the model coefficient of determination and residual sum of squared errors (r^2 = 0.55 ± 0.03, SSE = 4.6×10^6 ± 7.6×10^5 ppt^2). In scenario S2/S3, source S2 is shown to account for 25%and 6.7% of the nighttime and daytime budget, respectively, while source S3 accounts for 19% and 11% of the nighttime and daytime budget, respectively. However, despite improved model fit, there remains significant underestimation of daytime HONO; on average, a 0.15 ppt/s unknown daytime HONO source, or 67% of the total daytime source, is needed to bring scenario S2/S3 into agreement with observation. Estimates of 'best fit' parameterizations across lower to upper-limit values results in a moderate reduction of the unknown daytime source, from 0.15 to 0.10 ppt/s.

Keywords: air quality; unknown HONO source; Monte Carlo simulation; evolutionary solver

1. INTRODUCTION

Atmospheric nitrous acid (HONO) is important due to the role of HONO in generation of the hydroxyl radical (OH). There are a number of known sources of OH in the troposphere; however, OH production from HONO is of interest because the sources, fate, and diurnal cycling of HONO in the atmosphere have only recently begun to be elucidated. Models of atmospheric HONO generally employ a mass balance approach that allows evaluation of the HONO budget, often with a potentially limiting photostationary state assumption. As summarized by Spataro and Ianniello (2014) models generally include sources, sinks, and transport, the last relevant as formation processes hypothesized to occur at the ground result in vertical gradients of HONO.

Homogeneous and heterogeneous reactions, as well as direct emission of HONO from combustion sources, contribute to the presence of HONO in the troposphere (Finlayson-Pitts and Pitts, 1999). Nitrous acid strongly absorbs sunlight at wavelengths shorter than 390 nm resulting in photolytic degradation to OH and nitric oxide (NO). This results in suppressed, but non-zero, mixing ratios of daytime HONO due to the presence of daytime sources (Kleffmann, 2007). At night, the absence of this photolytic loss mechanism results in HONO accumulation, generally on the order of 0.1 ppb to 10 ppb (Kleffmann et al., 2003; Su et al., 2008; Young et al., 2012). The resumption of HONO photolysis after sunrise can lead to substantial formation of OH in the early morning. Alicke et al. (2003) report that during the BERLIOZ investigation at a rural, lightly trafficked site with low anthropogenic emissions during the summer months, photolysis of HONO was the dominant source of OH in the morning, and contributed as much as 20% of 24-h integrated OH production.

Modeling studies generally show the need for an unknown daytime source to close the HONO budget (Staffelbach et al., 1997; Lee et al., 2015). A number of photochemically driven

67 homogeneous reactions have been identified or considered: e.g., the known reaction of OH and
68 NO and the hypothesized reaction of photolytically excited nitrogen dioxide (NO_2) and water (Li
69 et al., 2008). The latter, however, may not proceed sufficiently rapidly or at adequate yields to
70 affect HONO mixing ratios in the atmosphere (Carr et al., 2009). Other potential homogeneous
71 sources are under discussion and review. For example, Li et al. (2014) proposed an internal
72 source of HONO that consumed nitrogen oxides, although follow up discussion and further
73 experiments indicate the source was likely strongly overestimated (Li et al., 2015; Ye et al.,
74 2015).

75 Nitrous acid formation mediated by aerosol surface area (SA) is a topic of ongoing
76 research, largely because the complexity of aerosols results in substantial uncertainty regarding
77 their ultimate role in HONO formation. Static surfaces such as the ground (Stemmler et al.,
78 2006) also may enhance HONO formation. Other hypothesized daytime sources include
79 emissions resulting from acid/base chemistry in soils (Su et al., 2011) and photolysis of nitric
80 acid (HNO_3) on forest canopy surfaces (Zhou et al., 2011). Photoenhanced conversion of NO_2 on
81 organic surfaces, including the ground and aerosols, are also thought to contribute to the daytime
82 HONO budget (George et al., 2005; Stemmler et al., 2006, 2007).

83 Given the many identified and proposed HONO source and sink mechanisms, single
84 value estimates of parameterizations of HONO sources and sinks limit the ability to understand
85 the impact of variability in multiple input parameters on models of HONO dynamics in the
86 atmosphere. Monte Carlo simulation (MCS) provides a tool to observe the combined effects of
87 ranges of input parameters and the resulting impact on the agreement between model output and
88 measurements. In this work, we identify fourteen HONO sources or sinks established in the
89 literature, including three sources that have recently (2013-2014) been identified. We evaluate

these recently identified sources through incorporation into a baseline model with a full-factorial, deterministic screening analysis. We then identify scenarios for which we stochastically parameterize source and sink mechanisms with MCS to determine probability distributions of modeled HONO mixing ratios.

2. METHODS

2.1 Measurements

Measurements of gas- and particle-phase constituents were made from May 30 to July 1, 2011 in a semi-urban area approximately 68 km northwest of the Dallas-Fort Worth (DFW) metropolitan area. The monitoring site was co-located with the Texas Commission on Environmental Quality Eagle Mountain Lake (EML) continuous ambient monitoring station (CAMS 75). Further details regarding the geography, surrounding industrial and biogenic activities, and site conditions have been outlined previously (Rutter et al., 2015)

Temperature, humidity (Vaisala, HMP-45C in a RM Young 10-plate solar radiation shield), and planetary boundary layer (PBL) height (Vaisala, CL31) were measured throughout the duration of the campaign. Mixing ratios of HONO and HNO_3 were measured every five minutes using a method that coupled a mist chamber with ion chromatography (Dionex, CD20-1), described in greater detail elsewhere (Dibb et al., 2004). First-order photolysis rate constants (*j*-values) were determined with radiometric measurements of actinic flux determined with a 2-pi double monochrometer with photomultiplier and subsequent calculations following IUPAC recommendations. Nitrogen oxides were recorded every minute using a chemiluminescence trace level NO-NO_2-NO_x analyzer (Thermo Electron Corp., Model 42C) equipped with a Blue Light Converter (Air Quality Design, Inc.) for NO_2 quantification. Hydroxyl radical was observed using atmospheric pressure chemical ionization mass spectrometry (Kim et al., 2013). One-hour

averaged mixing ratios of volatile organic compounds (VOCs) were measured using a thermal desorption gas chromatograph with flame ionization detection (Perkin-Elmer O_3 Precursor Analyzer System). Continuous measurements of number-based particle size distributions (diameter range of 20 nm to 500 nm) were made every ten minutes with a scanning electrical mobility sizer (SEMS, Brechtel Inc. Model 2002) and were converted to SA distributions assuming spherical particles. Concentrations of particulate phase nitrate were determined with an Aerodyne high-resolution time-of-flight aerosol mass spectrometer, as described by Rutter et al. (2015). Black carbon concentrations were measured using an aethalometer.

2.2 Baseline model

A two-layer box model describing HONO mixing ratios was developed, with the height of the first layer set to 36 m to represent a surface layer and the height of layer 2 set to 72 m to facilitate use of HONO observations above the surface layer that are available in the literature. Established source (labeled as 'B1-B8' in Table 1) and sink mechanisms (labeled 'L1-L3' in Table 1) are described in full in the Supporting Information (SI) (including Figures S1-S5 and equations S1-S20). The timeframe selected for continuous modeling was 22 June 01:00 to 25 June 14:00 (all times local) based on the longest uninterrupted period during the campaign with observations of HNO_3, HONO, aerosol SA, NO_2, NO, gas-phase chloride (assumed to be hydrochloric acid, HCl), and j_{HONO}. Mixing ratios of constituents during this period were generally typical of the broader study period. Equation 1 describes baseline sources and sinks modeled with a transient approach:

$$\frac{d[\mathrm{HONO}]_{trans}}{dt} = F_{B1} + F_{B2} + F_{B3} + F_{B5} + F_{B6} + F_{B7} + F_{B8} - \left(F_{L1} + F_{L2} + F_{L3}\right) - \Psi_{trans} \quad (1)$$

where $[HONO]_{trans}$ is the mixing ratio of HONO from modeled transient sources and sinks (ppt), *dt* is the time step (s) between measurements for which observations of all constituents present in Equation 1 were made, *F* represents the source or sink strength of the indicated mechanism (ppt/s), and Ψ_{trans} is the loss (or source) of HONO from layer 1 to (or from) layer 2 due to vertical transport (ppt/s).

Equation 1 describes the transient processes occurring in the model; source B4 was incorporated into the model after accounting for transient processes as shown in Equation 2:

$$[HONO]_{total} = [HONO]_{trans} + f_{emiss}\Delta[NO_x] \quad (2)$$

where $[HONO]_{total}$ is the mixing ratio of HONO at a time step resulting from transient and instantaneous processes (ppt) and f_{emiss} is the direct HONO emission factor described in Table 1. Equation 2 may overestimate the contribution of B4 in a box-model, as during the daytime, HONO will rapidly photolyze prior to the measurement of emitted NO_x.

Vertical transport, Ψ_{trans} (ppt/s), is calculated using a first-order flux-gradient relationship simulated with the 1D CACHE model (Bryan et al., 2012) where mass is transported by eddy diffusion at a magnitude proportional to the eddy diffusivity for heat (K_h), shown in equation 3:

$$\Psi_{trans} = -K_h(z,t)\frac{\partial C(z,t)}{\partial z}\frac{1}{h} \quad (3)$$

where $K_h(z,t)$ is the eddy diffusivity (m^2/s) at height *z* (m) and time *t.* As shown in equation 3, estimates of flux are divided by *h*, the height of the second layer in the model (m), prior to inclusion in equation 1.

Two 1D simulations during the campaign were used to derive K_h, including one simulation for 7-9 June and one for 10-12 June. For the layers corresponding to the upper boundary that are used in the results here, K_h is derived based on a length scale, vertical wind

shear, and a stability parameter (Forkel et al., 1990). It is calculated at each time step within the model, providing a diurnal cycle that is based on meteorological conditions during the campaign.

Observations of HONO were made at one elevation, approximately 10 m above surface, and were used to represent the HONO mixing ratio in layer 1 of the model. Equation 3 requires an estimate of the HONO mixing ratio in layer 2 to estimate the HONO gradient. Three scenarios were considered: 1) no gradient (i.e., [HONO] in layer 1 equals that in layer 2 at all times); 2) a gradient created using fractions of [HONO] presented in Vandenboer et al. (2013), representative of a stronger nighttime gradient and a weaker daytime gradient (GrN); and 3) a gradient created from fractions of [HONO] presented in Villena et al. (2011) that is representative of a stronger daytime gradient and weaker nighttime gradient (GrD). Diurnal profiles of the three gradient conditions are shown in Figure S6 of the SI and implications of this limitation are discussed in Section 3.2.

2.3 Parameterization and evaluation of newly identified HONO sources

Three recently identified HONO source mechanisms were parameterized to assess the potential of these mechanisms (in conjunction with B1-B8 and L1-L3) to independently or jointly account for HONO mixing ratios observed in DFW. The three mechanisms, listed in Table 1 as S1, S2, S3 are incorporated into Equation 1 as additional sources of HONO.

Source S1 is the formation of HONO from the reduction of HNO_3 to HONO mediated by VOCs emitted from motor vehicles (Rutter et al., 2014). The source strength (F_{S1}, ppt/s) was parameterized using HONO source strength and reactant mixing ratios presented in Table 1 of Rutter et al. (2014) and is shown in equation 4:

$$F_{S1} = f_{HNO_3,VOC}\left[\frac{\left(\frac{[\text{Propylene}]}{[\text{Benzene}]}\right)_{EML}}{\left(\frac{[\text{Propylene}]}{[\text{Benzene}]}\right)_{Max,DFW}}\right]\left[\frac{[\text{HNO}_3]_{\text{EML}}}{[\text{HNO}_3]_{\text{rutter}}}\right] \quad (4)$$

where $f_{HNO3,VOC}$ is the observed HONO formation rate (ppt s^{-1}) in Rutter et al. (2014), and normalizing ratios are further described in the SI. Estimates of 'likely' $f_{HNO3,VOC}$ were taken for experiments conducted at 50% RH while 'lower-limit' and 'upper-limit' estimates were taken as the minimum and average across experiments shown in Table 1 of Rutter et al. (2014). Normalizing assumptions shown in equation 4 resulted in, on average, ~95% reduction of $f_{HNO3,VOC}$ when calculating $F_{S1.}$ The form of the parameterization in equation 4 is speculative; propylene is chosen as a proxy for reactive VOCs while benzene is chosen to account for dilution that may occur as air masses move from DFW to EML (see Figure S7 in the SI for a diurnal profile of propylene/benzene). Identification of specific reactive species participating in the HONO formation process identified in Rutter et al. (2014) would enable improvements in development and assessment of parameterizations of VOC-mediated conversion of HNO_3 to HONO.

Source S2 is HONO emissions from soil bacteria as described by Oswald et al. (2013). Emission from the soil (F_{S2}, ppt/s) was assumed to mix instantaneously through the first model layer as shown in equation 5:

$$F_{S2} = \frac{f_{soil}}{h}\Gamma_{S2} \quad (5)$$

where f_{soil} is the "optimum" HONO flux from a soil type (molec cm^{-2} s^{-1}), h is the height of the model layer, and Γ_{S2} represents the conversion factor to ppt/s prior to inclusion in equation 1 (see the SI equations S21-S24 for an example calculation). The 'lower-limit' value of f_{soil} was taken

192 as the value of HONO flux for pasture, and the 'upper-limit' value was taken as that for
193 grassland. No 'likely' value of f_{soil} was selected, as pasture and grassland were the only two
194 relevant soil types for the DFW region. Despite specifying a 'lower-limit' value, this
195 investigation may be effectively considering the high end of contribution of soil bacteria to
196 HONO because "optimum" values of flux are used for both soil types.

197 Source S3 is the re-emission of HONO from a surface nitrite reservoir by displacement
198 from HNO_3 and HCl, as in Vandenboer et al. (2014, 2015) and shown in equation 6:

$$F_{S3} = \frac{[HNO_3] + [HCl]}{h} v_d \eta \quad (6)$$

199 where F_{S3} is the source strength of S3 (ppt s^{-1}), v_d is the deposition velocity of HNO_3 and HCl,
200 taken as 1 cm s^{-1}, and η is the displacement efficiency, ranging from 1% to 9% to 20% for
201 'lower-limit', 'likely', and 'upper-limit' values, respectively (VandenBoer et al., 2014). This
202 parameterization was constrained by the calculation of a 'reservoir' of nitrite from deposited
203 HONO, approximated from a material balance on the ground where the source of nitrite is
204 mechanism L1 and loss is due to displacement from mechanism S3. Mechanism S3 was set to 0
205 when the reservoir was equal to 0. As there may be additional sources of surface nitrite other
206 than gas-phase HONO and surface nitrite accumulation over greater than diurnal time-scales,
207 equation 6 likely represents a conservative estimate of the source strength of S3. Further
208 description of the constraints on source S3 is given in the SI and dynamics are depicted in Figure
209 S8, also in the SI.

210 *2.4 Model calculation and assessment*

211 Nitrous acid mixing ratios were first modeled with the baseline scenario using the B and
212 L parameterizations summarized in Table 1. The 'likely' parameterization incorporates HONO

source and sink estimations thought most representative of each mechanism, while 'upper-limit' and 'lower-limit' are values that result in maximum or minimum HONO production, respectively, e.g. in the 'upper-limit', parameterizations of sources result in greater formation while those of sinks result in lower loss rates. Predictions of HONO mixing ratios were assessed through the residual sum of squared errors (SSE) and the coefficient of determination (r^2), both determined from differences between modeled and measured HONO mixing ratios.

Model scenarios were constructed to assess the three new mechanisms (mechanism ID = S1, S2, and S3 shown in Table 1) and gradient conditions (GrN or GrD); scenarios are named according to the gradient used and sources added, e.g., GrN S2/S3 refers to a model scenario with the stronger nighttime gradient as described previously and with sources S2 and S3 added to baseline sources B1-B8 and sinks L1-L3. Sources S1-S3 were added to the baseline model in a full-factorial deterministic screening analysis (using 'likely' estimates of parameterizations) to identify scenarios for further analysis. Monte Carlo simulation (Crystal Ball v. 11.1.2.3, Oracle) was used to evaluate the probability of model scenarios to account for observed HONO mixing ratios. Input distributions of source and sink parameterizations were assumed to be triangular probability distributions, bounded by 'lower-limit' and 'upper-limit' values with the 'likely' value as the most frequently occurring. Model sensitivity to the number of trial simulations was performed to ensure a trial-independent solution was achieved; all MCS were conducted with 5,000 iterations. A bounded evolutionary solver was applied to the baseline model scenario and to the model scenario with the highest r^2 and lowest residual SSE in the deterministic screening analysis. The evolutionary solver used a genetic algorithm to estimate source and sink parameterizations with a minimum SSE across the range of 'lower-limit' to 'upper-limit' values for each source or sink mechanism.

3. RESULTS AND DISCUSSION

3.1 Ambient air monitoring in the outflow of DFW

Experimental observations of mixing ratios of ambient gases and particles input to the model are shown in Figure 1; diurnal profiles of selected constituents across the full monitoring campaign are shown in Figure S9 of the SI. Values of $HONO/NO_2$ are variable and elevated during the daytime, possibly indicative of a secondary daytime source of HONO. Mixing ratios of HNO_3 are suppressed in the morning and evenings and elevated during daytime hours, likely a result of strong daytime HNO_3 production from the reaction of NO_2 and OH (Aneja et al., 1994). The highest observed mixing ratios of HNO_3 across the full monitoring campaign are included in the model period shown in Figure 1, exceeding 5000 ppt in the early evening of June 22, 2011. Mixing ratios of HCl exhibit similar trends to those observed for HNO_3. Mixing ratios of HONO show accumulation over the nighttime and suppression during the daytime, a result of the strong loss due to photolysis and convective dilution during the daytime hours. Aerosols and aerosol-phase constituents appear elevated during the nighttime hours of 6/23 and 6/24 compared to daytime concentrations, but are suppressed during the nighttime of 6/25. Across the model period, the SA of particulate matter averages 125 $\mu m^2\ cm^{-3}$, consistent with typical values across the month-long monitoring campaign (Figure S1), and ranges 22 $\mu m^2\ cm^{-3}$ - 392 $\mu m^2\ cm^{-3}$.

3.2 Baseline model

Mixing ratios of HONO are first calculated with the model under the baseline scenario for 'likely' estimates of parameterizations. Predicted and measured mixing ratios of HONO for the baseline scenario with three HONO gradient conditions described in Section 2.2 are shown in Figure 2. The "no gradient" condition results in substantial over-estimation of nighttime HONO mixing ratios, logical given the role of the ground surface in HONO formation processes

included in the baseline scenario and the first layer height of 36 m. Conversely, the GrN and GrD conditions both result in underestimation of nighttime HONO, with relatively small differences between the two conditions. A strong daytime sink, due to photolysis, results in suppression of modeled daytime mixing ratios below observation for all three gradient conditions, implying the need for daytime sources beyond those considered in the baseline scenario. The underestimation may also result from the limited vertical resolution in the two-layer box model used here and the measurement height in the lower portion of the first layer (10 m); it is likely that a continuous HONO gradient is present in the 36 m of the model first layer resulting in a lower modeled mixing ratio across the first model layer than the 10 m observation.

While relatively few studies report measurements of vertical gradients of HONO, available profiles generally show higher HONO mixing ratios in surface layers than aloft, indicative of ground surface HONO formation. Michoud et al. (2014) summarize several studies reporting vertical gradients, four of which show the presence of a vertical gradient (Veitel, 2002; Zhang et al., 2009; Villena et al., 2011; Wong et al., 2012) and one that does not (Häseler et al., 2009). Vandenboer et al. (2013) report high-resolution vertical profiles measured from a tower in Boulder, CO, and show the presence of both daytime and nighttime HONO gradients. Veitel et al. (2002) report that over 13 months of measurements, HONO mixing ratios were observed to decrease with height under nearly all atmospheric conditions. For the present investigation, we interpret the over-prediction of HONO mixing ratios in the nighttime for the "no gradient" condition, when convective mixing is most likely to be diminished, to indicate a HONO vertical gradient. Thus, conditions GrN or GrD better represent the vertical structure of HONO mixing ratios in the outflow of DFW. While this appears to be in agreement with the preponderance of available HONO vertical gradient measurements, a site-specific HONO gradient would clearly

improve the present study. Nevertheless, parameterizations here allow an estimation of the source and sink processes in the outflow of DFW and exploration of two estimates of gradients to assess model sensitivity to the HONO vertical profile. The impact of the vertical gradient and of parameterizations of established and recently identified HONO sources and sinks are further explored in Sections 3.3-3.5.

3.3 Deterministic screening analysis

A deterministic screening analysis was employed to evaluate model outcomes when sources S1-S3, acting independently or in any combination, are incorporated into the model. This full-factorial analysis, consisting of 24 possible scenarios, is conducted for only the 'likely' parameterizations of the mechanisms, as shown in Table S1 of the SI. Full output of model runs across all gradient conditions and scenarios of parameterizations are provided in Figures S10-S12.

Generally, 'likely' estimates of parameterizations showed improved model fit compared to 'upper-limit' estimates, implying additional sources of HONO, rather than increased production from baseline sources result in improved model outcomes. Subsequent discussion in this section reflects 'likely' parameterizations. Scenarios identified for further investigation are those with a combination of low SSE and high r^2. The baseline model generally is characterized by the highest model SSE, and the addition of source mechanisms S1-S3 generally lowers SSE and increases r^2. In cases, however, the SSE is lowered while the r^2 decreases (for example, from GrN Baseline to GrN S1). This is a result of improvement in model prediction for only a subset of times in the modeling period. The screening analysis identified scenario S2/S3 and scenario S1/S2/S3 as having the lowest SSE and highest r^2 (SSE range: 4.3×10^6–6.7×10^6; r^2 range: 0.42-

304 0.58). These scenarios, along with baseline scenarios for comparison, are further explored with
305 MCS and an evolutionary solver.

306 *3.4 Monte Carlo simulation*

307 Six model scenarios that vary the new sources and vertical gradient conditions were
308 evaluated with MCS to incorporate uncertainty and variability in each mechanism into the
309 model; model estimates of HONO are determined as probabilistic distributions at each model
310 time step. Summarized output of MCS are shown in Figure 3 as hourly-averaged diurnal profiles
311 of measured and modeled distributions of HONO mixing ratios across the model period. The
312 MCS reinforces the conclusions that 'baseline' source mechanisms cannot explain observed
313 HONO mixing ratios; in the GrN Baseline condition, 90^{th} percentile values of model output
314 underestimate observed HONO mixing ratios in 23 of 24 reported hours, and 75^{th} percentile
315 values underestimate observed HONO mixing ratios all 24 reported hours.

316 The addition of source mechanisms S2 and S3 to the model (Figure 3) results in
317 improved agreement between the model and observations for nighttime mixing ratios of HONO
318 for both GrN and GrD conditions. GrN S2/S3 shows 9 of the 10 hours in the 21:00-07:00
319 nighttime period are between the 10^{th} and 90^{th} percentile values determined in the model. GrD
320 S2/S3 shows improvement over the GrD Baseline condition; however, metrics of goodness of fit
321 are lower than GrN S2/S3, and there is less improvement over baseline. This appears to be a
322 result of sustained accumulation over the nighttime period, due to the smaller HONO nighttime
323 vertical gradient in the GrD condition. Under both GrN and GrD conditions for scenario S2/S3,
324 daytime mixing ratios of HONO remain substantially underpredicted as in the baseline condition.

The addition of all three sources (S1, S2, and S3) does not appear to resolve underprediction of the daytime HONO mixing ratio. In the GrN condition, the addition of source S1 results in a small increase in over-estimation of nighttime HONO mixing ratios and metrics of model fit worsen. In the GrD condition, there is a limited impact from the combined effect of sources S1, S2 and S3, with a modest reduction in both SSE and correlation coefficient when comparing GrD S1/S2 to GrD S1/S2/S3. Figure 3 shows GrN S2/S3 results in improved model fit compared to other scenarios, although daytime HONO remains substantially underestimated.

An estimation of average total and relative source and sink strength across both nighttime (21:00 – 07:00) and daytime (07:00 – 21:00) is shown in Figure 4 for GrN S2/S3. Estimates of sources and sinks are reported for 'likely' values of parameterizations for the indicated time period. Considerable temporal differences in the contributions of various source and sinks to the HONO budget exist. At night, HONO from NO_2 conversion at the ground (B7) is the major source, contributing 53% of the HONO budget. Biotic release from the ground (S2) and re-emission from the nitrite reservoir (S3) are the next two largest contributors at 25% and 19%, respectively. Nighttime HONO is slightly over-estimated; an 'unknown' nighttime sink of 0.0016 ppt/s, or 3% of the total, is required to bring the model into agreement with observations. Major nighttime sinks are vertical transport and deposition of HONO at the ground surface, contributing 73% and 21%, respectively. These nighttime sources and sinks are in general agreement with relative estimates of mechanisms reported by Czader et al. (2012), who report 71% of HONO production due to heterogeneous surface chemistry and losses due to transport and deposition of 77% and 23%, respectively, during the nighttime and pre-sunrise morning.

During the daytime, a missing HONO source dominates; however there are meaningful contributions to the daytime HONO budget from S3, S2, B8, B7 and B5. A missing daytime

source of 0.15 ppt s^{-1}, or 67% of the total HONO source budget shown in Figure 4, is needed to bring modeled and measured results into full agreement. This "missing" source is in the range of magnitudes identified in other investigations, ranging from 0.03 - 0.3 ppt s^{-1} (Su et al., 2008; Elshorbany et al., 2009; Sörgel et al., 2011; VandenBoer et al., 2013; Lee et al., 2015). Unless there is a positive artifact that depends on sunlight, a strong daytime source is needed to balance the substantial sink of HONO due to photolysis (89% of the total sink). In section 3.5, we explore the potential for 'best fit' estimates of parameterizations in GrN S2/S3 to close some portion of the HONO budget through optimization of parameterizations across the range of values presented in Table 1.

3.5 Evolutionary solver and sensitivity analysis

An evolutionary solver was employed to estimate the optimal combination of input values within 'lower-limit' to 'upper-limit' ranges of parameterizations and the resulting impact on the estimate of the "missing" HONO source or sink. The evolutionary solver was applied to the GrN baseline scenario and GrN S2/S3. Model outcomes with optimal estimates for GrN baseline and GrN S2/S3 are shown in Figure 5 and parameterizations are reported in Table 2.

Across optimization of both GrN Baseline and GrN S2/S3, the largest changes to the parameterizations relate to heterogeneous conversion of NO_2 on aerosol (B1 and B2) and on the ground (B7, B8), and HONO uptake to the ground (L1). Aerosol processes increase substantially as a result of a speculative upper-limit as described in the SI; B1 was allowed to vary over 1.5 orders of magnitude and B2 over 2.5 orders of magnitude based on prior modeling studies, rather than experimental estimates. However, contributions from B1 and B2 remain limited (< 1% as can be determined from absence of B1 and B2 in Figure 4), in part a result of the two layer box-model used here that emphasizes ground-level phenomena. In both GrN Baseline and GrN

S2/S3, the optimization resulted in B8 at the upper-limit of the parameterization. Source B7 increased by ~2× in GrN Baseline, but more moderately in GrN S2/S3, a result of the contribution of sources S2 and S3 in GrN S2/S3. In GrN S2/S3, deposition loss (L1) increased, a result of the need to balance increases in parameterizations of sources that act over both daytime and nighttime periods (e.g., S3) and contribute to reductions in the daytime "unknown" source but also nighttime accumulation.

Figure 5 shows greater improvements in metrics of model goodness of fit for the optimal solution of GrN S2/S3 compared to the optimal solutions of the GrN Baseline. This indicates that baseline mechanisms are not able to similarly explain HONO observations under any combination of input parameters compared to the scenario with S2/S3 present. This appears to largely result from stronger parameterizations of S2/S3 resulting in improved estimates of daytime HONO mixing ratio, although levels are still lower than observed. Best-fit parameterizations of GrN S2/S3 result in a missing daytime source of 0.10 ppt/s, reduced from 0.15 ppt/s (Figure 4), implying that a substantial missing HONO source remains even across a statistically optimized range of parameterizations.

The "best-fit" estimates of GrN S2/S3 reflect an improved statistical outcome for the model when parameterizations are allowed to vary across a range of values. Parameterizations in Table 2 with larger percentage changes imply a combination of model sensitivity to the parameter as well as uncertainty in the value of the parameterization. We conducted a sensitivity analysis to identify the most important parametrizations impacting the estimates of goodness-of-fit, the model r^2 and SSE. The sensitivity analysis for GrN S2/S3 is summarized in Table S2 of the SI, reported as the Spearman's rank correlation coefficient (ρ) between each mechanism's input parameter and the model output r^2 or SSE. Uptake of NO_2 at the ground (B7) is the

parameter with the largest impact on both the model SSE and r^2, by a comparatively large margin. Given that there is a wide range of estimates of the uptake coefficient parameterizing B7 in the literature, this source represents a large source of uncertainty in the model. Sources S3, B8, and S2 are the next three strongest correlations with model SSE; interestingly, all four sources with highest sensitivity (B7, B8, S2, and S3) are ground-level phenomena. Source B7 was strongest correlated with night-time (21:00-07:00) HONO mixing ratios while source S3 was strongest correlated with daytime HONO. This underscores the importance of characterizing the role of the ground surface mechanisms, including biotic release and ground-level chemical transformations.

The presence of a substantial missing daytime source is further explored via estimation of correlation coefficients between measured constituents and products of constituents with the missing HONO source, similar to the analysis presented by Lee et al. (2015). This analysis employed time-series measurements for constituents and the estimate of missing HONO at each time step required for model agreement with observation. Outcomes are shown in Table S3 for 'likely' and 'best-fit' estimates of GrN S2/S3. Relatively strong correlation coefficients ($r^2 > 0.5$) were observed for j_{NO2} and j_{NO2} × temperature with the missing HONO source, the latter in close agreement to the results of Lee et al (2015). However, the correlation of $j_{NO2} \times NO_2$ with the missing HONO source is weak (r^2 = 0.09 - 0.17), as is the correlation of j_{NO2} × SEMS SA× NO_2 (r^2 = 0.08 - 0.16) and with NO_2 alone (r^2 = 0.21-0.25). The stronger correlation with j_{NO2} and j_{NO2} × temperature may imply photosensitized conversion on organics, including humic acids, which are mainly ground surface sources (Stemmler et al., 2006, 2007), are underestimated. The weak correlation of the missing HONO source with NO_2 and products containing NO_2 mixing ratios appears aligned with a recent analysis of weekday-weekend HONO and NO_2 relationships

that shows HONO production rates do not increase with increases in NO_2, implying daytime HONO production may not be rate-limited by NO_2 (Pusede et al., 2015). Weakening correlations for products of gas- and particle-phase constituents and j_{NO2} also may result from the two-layer model that lends greater emphasis to interactions at the ground level, consistent with the results of the sensitivity analysis in Table S2 and discussed previously.

3.6 Model limitations

The model described in this work is subject to a number of important limitations. Source S1 assumes the source strength determined in the laboratory is possible in the ambient environment, with several normalizing assumptions. However, as we did not observe meaningful formation of HONO from source S1, the impact of the speculative parameterization is therefore limited in this investigation. Future field efforts should further investigate the potential for VOC-mediated reduction of HNO_3 to HONO in near-source environments. Source S2 was parameterized using a single value for a model simulation; there are likely to be diurnal variations in biological activity and soil water content that would impact the parameterization of source S2. Source S3 considered only gas-phase HONO as an input to the surface nitrite reservoir and that the reservoir was empty at the beginning of the model period. This may result in a conservative estimate of the contribution of source S3.

Input distributions in MCS were assumed to be triangular. This assumption may over-weight estimates of parameterizations at the 'upper-limit' and 'lower-limit' extents of the distribution as compared to a normal distribution. A triangular distribution was chosen, in part, to ensure parameterizations did not exceed upper or lower-limit estimates in MCS. The two-layer box model uses instantaneous and *in-situ* mixing ratios to constrain the model, with the assumption of instantaneous mixing up to the first layer height. Transport between layers was

estimated using an approximation of HONO vertical gradients at similar heights taken from literature. We assume transport time for NO_x sources that exceeds the atmospheric age of HONO (Lee et al. 2013). During the daytime periods (07:00-21:00), the atmospheric age of HONO across the modeling period in this work averaged 19.4 min and ranged from 8.9 to 128 min. We assume NO_x sources input to the model originate from the metropolitan DFW area (~70 km away), while the wind speed averaged 19 km/h, resulting in a transport time of 220 min.

4. CONCLUSIONS

Model predictions of HONO that account for ranges in parameterizations of HONO source and sink mechanisms enable a statistical assessment of the likelihood of the model to match observation. Observations of HONO appear most accurately simulated when emission from soil biota (S2) and re-emission from a ground level nitrite source (S3) are included in the model. Model output for GrN S2/S3 accounted for, on average, 33% of the daytime HONO budget and 103% of the nighttime HONO budget. Major nighttime sources included (in order) NO_2 conversion at the ground (B7), biotic release from soil (S2), and re-emission from the nitrite reservoir (S3). Major daytime sources include S3, S2, photoenhanced NO_2 conversion at the ground (B8), B7, and the reaction of OH with NO (B5). Model fit improved after application of an evolutionary solver, resulting in a reduction of the estimate of the unknown daytime source for GrN S2/S3. However, the presence of a substantial unknown daytime source (on average 0.10 ppt/s) even with a statistically optimal fit for GrN S2/S3 implies additional sources of HONO than those evaluated here must be included to reproduce accurately daytime HONO mixing ratios. Analyses of model sensitivity and correlations between the missing HONO source and constituents imply the presence of additional, or underestimation of considered, ground-level HONO sources in this investigation.

ACKNOWLEDGEMENTS

The support of the Texas Commission on Environmental Quality Air Quality Research Program is gratefully acknowledged. We also thank the two reviewers whose comments and suggestions greatly improved the model and manuscript.

REFERENCES

Alicke, B., Geyer, A., Hofzumahaus, A., Holland, F., Konrad, S., Pätz, H-W. et al.. OH formation by HONO photolysis during the BERLIOZ experiment. J. Geophys. Res. Atmos. 108 (D4), 8247.

Aneja, V.P., Claiborn, C.S., Li, Z., Murthy, A., 1994. Trends, seasonal variations, and analysis of high-elevation surface nitric acid, ozone, and hydrogen peroxide. Atmospheric Environment 28, 1781–1790.

Aumont, B., Chervier, F., Laval, S., 2003. Contribution of HONO sources to the NOx/HOx/O3 chemistry in the polluted boundary layer. Atmospheric Environment 37, 487–498.

Bryan, A.M., Bertman, S.B., Carroll, M.A., Dusanter, S., Edwards, G.D., Forkel, R. et al., 2012. In-canopy gas-phase chemistry during CABINEX 2009: sensitivity of a 1-D canopy model to vertical mixing and isoprene chemistry. Atmos. Chem. Phys. 12, 8829–8849.

Carr, S., Heard, D.E., Blitz, M.A., 2009. Comment on "Atmospheric Hydroxyl Radical Production from Electronically Excited NO2 and H2O." Science 324, 336b.

Dibb, J.E., Scheuer, E., Whitlow, S.I., Vozella, M., Williams, E., Lerner, B.M., 2004. Ship-based nitric acid measurements in the Gulf of Maine during New England Air Quality Study 2002. J. Geophys. Res. Atmos. 109, D20303.

Elshorbany, Y.F., Kurtenbach, R., Wiesen, P., Lissi, E., Rubio, M., Villena, G. et al., 2009. Oxidation capacity of the city air of Santiago, Chile. Atmospheric Chemistry and Physics 9, 2257–2273.

Finlayson-Pitts, B.J., Pitts, J., 1999. Chemistry of the upper and lower atmosphere: Theory, experiments, and applications. Academic Press.

Forkel, R., Seidl, W., Dlugi, R., Deigele, E., 1990. A one-dimensional numerical model to simulate formation and balance of sulfate during radiation fog events. J. Geophys. Res. 95, 18501–18515.

George, C., Strekowski, R.S., Kleffmann, J., Stemmler, K., Ammann, M., 2005. Photoenhanced uptake of gaseous NO_2 on solid organic compounds: a photochemical source of HONO? Faraday Discuss. 130, 195–210; discussion 241–264, 519–524.

Häseler, R., Brauers, T., Holland, F., Wahner, A., 2009. Development and application of a new mobile LOPAP instrument for the measurement of HONO altitude profiles in the planetary boundary layer. Atmos. Meas. Tech. Discuss. 2, 2027–2054.

Kim, S., Wolfe, G.M., Mauldin, L., Cantrell, C., Guenther, A., Karl, T. et al., 2013. Evaluation of HOx sources and cycling using measurement-constrained model calculations in a 2-methyl-3-butene-2-ol (MBO) and monoterpene (MT) dominated ecosystem. Atmos. Chem. Phys. 13, 2031–2044.

Kirchstetter, T.W., Harley, R.A., Littlejohn, D., 1996. Measurement of nitrous acid in motor vehicle exhaust. Environ. Sci. Technol.30, 2843–2849.

Kleffmann, J., 2007. Daytime sources of nitrous acid (HONO) in the atmospheric boundary layer. Chemphyschem 8, 1137–1144.

Kleffmann, J., Becker, K.H., Wiesen, P., 1998. Heterogeneous NO_2 conversion processes on acid surfaces: possible atmospheric implications. Atmospheric Environment 32, 2721–2729.

Kleffmann, J., Kurtenbach, R., Lörzer, J., Wiesen, P., Kalthoff, N. et al., 2003. Measured and simulated vertical profiles of nitrous acid—Part I: Field measurements. Atmospheric Environment 37, 2949–2955.

507 Kurtenbach, R., Becker, K.H., Gomes, J.A.G., Kleffmann, J., Lörzer, J.C., Spittler, M. et al., 2001.
508 Investigations of emissions and heterogeneous formation of HONO in a road traffic tunnel.
509 Atmospheric Environment 35, 3385–3394.
510 Lee, J.D., Whalley, L.K., Heard, D.E., Stone, D., Dunmore, R.E., Hamilton, J.F., Young, D.E., Allan,
511 J.D., Laufs, S., Kleffmann, J., 2015. Detailed budget analysis of HONO in central London reveals
512 a missing daytime source. Atmos. Chem. Phys. Discuss. 15, 22097–22139.
513 Lee, B.H., Wood, E.C., Herndon, S.C., Lefer, B.L., Luke, W.T., Brune, W.H. et al., 2013. Urban
514 measurements of atmospheric nitrous acid: A caveat on the interpretation of the HONO
515 photostationary state. J. Geophys. Res. Atmos. 118, 12274-12281.
516 Li, S., Matthews, J., Sinha, A., 2008. Atmospheric hydroxyl radical production from electronically
517 excited NO2 and H2O. Science 319, 1657–1660.
518 Li, X., Rohrer, F., Hofzumahaus, A., Brauers, T., Häseler, R., Bohn, B. et al., 2014. Missing Gas-Phase
519 Source of HONO Inferred from Zeppelin Measurements in the Troposphere. Science 344, 292–
520 296.
521 Li, X., Rohrer, F., Hofzumahaus, A., Brauers, T., Häseler, R., Bohn, B. et al., 2015. Response to
522 Comment on "Missing gas-phase source of HONO inferred from Zeppelin measurements in the
523 troposphere." Science 348, 1326e.
524 Michoud, V., Colomb, A., Borbon, A., Miet, K., Beekmann, M., Camredon, M., et al. 2014. Study of the
525 unknown HONO daytime source at a European suburban site during the MEGAPOLI summer
526 and winter field campaigns. Atmos. Chem. Phys. 14, 2805–2822.
527 Monge, M.E., D'Anna, B., Mazri, L., Giroir-Fendler, A., Ammann, M., Donaldson, D.J., George, C.,
528 2010. Light changes the atmospheric reactivity of soot. PNAS 107, 6605–6609.
529 NASA, 2011. Chemical Kinetics and Photochemical Data for Use in Atmospheric Studies (No. JPL 10-
530 6). California Institute of Technology, Pasadena, CA, Jet Propulsion Laboratory.
531 Oswald, R., Behrendt, T., Ermel, M., Wu, D., Su, H., Cheng, Y. et al., 2013. HONO emissions from soil
532 bacteria as a major source of atmospheric reactive nitrogen. Science 341, 1233–1235.
533 Pusede, S.E., VandenBoer, T.C., Murphy, J.G., Markovic, M.Z., Young, C.J., Veres, P.R. et al., 2015. An
534 Atmospheric Constraint on the NO_2 Dependence of Daytime Near-Surface Nitrous Acid
535 (HONO). Environ. Sci. Technol. doi:10.1021/acs.est.5b02511
536 Rutter, A.P., Griffin, R.J., Cevik, B.K., Shakya, K.M., Gong, L., Kim, S., Flynn, J.H., Lefer, B.L., 2015.
537 Sources of air pollution in a region of oil and gas exploration downwind of a large city.
538 Atmospheric Environment. 120, 89–99.
539 Rutter, A.P., Malloy, Q.G.J., Leong, Y.J., Gutierrez, C.V., Calzada, M., Scheuer, E., Dibb, J.E., Griffin,
540 R.J., 2014. The reduction of HNO3 by volatile organic compounds emitted by motor vehicles.
541 Atmospheric Environment 87, 200–206.
542 Sörgel, M., Regelin, E., Bozem, H., Diesch, J.-M., Drewnick, F., Fischer, H. et al., 2011. Quantification
543 of the unknown HONO daytime source and its relation to NO_2. Atmospheric Chem. Phys. 11,
544 10433–10447.
545 Spataro, F., Ianniello, A., 2014. Sources of atmospheric nitrous acid: State of the science, current research
546 needs, and future prospects. J. Air Waste Manage. Assoc. 64, 1232–1250.
547 Staffelbach, T., Neftel, A., Horowitz, L.W., 1997. Photochemical oxidant formation over southern
548 Switzerland, 2. Model results. Journal of Geophysical Research 102, 23363-23373.
549 Stemmler, K., Ammann, M., Donders, C., Kleffmann, J., George, C., 2006. Photosensitized reduction of
550 nitrogen dioxide on humic acid as a source of nitrous acid. Nature 440, 195–198.
551 Stemmler, K., Ndour, M., Elshorbany, Y., Kleffmann, J., D'Anna, B., George, C.,et al., 2007. Light
552 induced conversion of nitrogen dioxide into nitrous acid on submicron humic acid aerosol.
553 Atmospheric Chem. Phys. 7, 4237–4248.
554 Su, H., Cheng, Y.F., Cheng, P., Zhang, Y.H., Dong, S., Zeng, L.M. et al, 2008. Observation of nighttime
555 nitrous acid (HONO) formation at a non-urban site during PRIDE-PRD2004 in China.
556 Atmospheric Environment 42, 6219–6232.

Su, H., Cheng, Y., Oswald, R., Behrendt, T., Trebs, I., Meixner, F.X., et al., 2011. Soil nitrite as a source of atmospheric HONO and OH radicals. Science 333, 1616–1618.

Trick, S., 2004. Formation of Nitrous Acid on Urban Surfaces - A physical-chemical Perspective. Dissertation. Universität Heidelberg, 2004, http://www.ub.uni-heidelberg.de/archiv/ 4814.

VandenBoer, T.C., Brown, S.S., Murphy, J.G., Keene, W.C., Young, C.J., Pszenny, A. A. P. et al., Roberts, J.M., 2013. Understanding the role of the ground surface in HONO vertical structure: High resolution vertical profiles during NACHTT-11. J. Geophys. Res. Atmos. 118, 10155–10171.

VandenBoer, T.C., Markovic, M.Z., Sanders, J.E., Ren, X., Pusede, S.E., Browne, E.C. et al., 2014. Evidence for a nitrous acid (HONO) reservoir at the ground surface in Bakersfield, CA, during CalNex 2010. J. Geophys. Res. Atmos. 119, 9093-9106.

VandenBoer, T.C., Young, C.J., Talukdar, R.K., Markovic, M.Z., Brown, S.S., Roberts, J.M., Murphy, J.G., 2015. Nocturnal loss and daytime source of nitrous acid through reactive uptake and displacement. Nature Geosci. 8, 55–60.

Veitel, H., 2002. Vertical Profiles of NO_2 and HONO in the Planetary Boundary Layer [WWW Document]. URL http://archiv.ub.uni-heidelberg.de/volltextserver/2490/ (accessed 10.6.15).

Villena, G., Kleffmann, J., Kurtenbach, R., Wiesen, P., Lissi, E., Rubio, M.A. et al., 2011. Vertical gradients of HONO, NOx and O3 in Santiago de Chile. Atmospheric Environment 45, 3867–3873.

Walcek, C.J., Brost, R.A., Chang, J.S., Wesely, M.L., 1986. SO_2, sulfate and HNO_3 deposition velocities computed using regional landuse and meteorological data. Atmospheric Environment 20, 949–964.

Wong, K.W., Tsai, C., Lefer, B., Grossberg, N., Stutz, J., 2013. Modeling of daytime HONO vertical gradients during SHARP 2009. Atmos. Chem. Phys.13, 3587–3601.

Wong, K.W., Tsai, C., Lefer, B., Haman, C., Grossberg, N., Brune, W.H. et al., 2012. Daytime HONO vertical gradients during SHARP 2009 in Houston, TX. Atmos. Chem. Phys. 12, 635–652.

Ye, C., Zhou, X., Pu, D., Stutz, J., Festa, J., Spolaor, M. et al., 2015. Comment on "Missing gas-phase source of HONO inferred from Zeppelin measurements in the troposphere." Science 348, 1326-d.

Young, C.J., Washenfelder, R.A., Roberts, J.M., Mielke, L.H., Osthoff, H.D., Tsai, C. et al., 2012. Vertically resolved measurements of nighttime radical reservoirs in Los Angeles and their contribution to the urban radical budget. Environ. Sci. Technol. 46, 10965–10973.

Zhang, N., Zhou, X., Shepson, P.B., Gao, H., Alaghmand, M., Stirm, B., 2009. Aircraft measurement of HONO vertical profiles over a forested region. Geophys. Res. Lett. 36, L15820.

Zhou, X., Gao, H., He, Y., Huang, G., Bertman, S.B., Civerolo, K., Schwab, J., 2003. Nitric acid photolysis on surfaces in low-NOx environments: Significant atmospheric implications. Geophysical Research Letters 30(23), 2217.

Zhou, X., Zhang, N., TerAvest, M., Tang, D., Hou, J., Bertman, S. et al., 2011. Nitric acid photolysis on forest canopy surface as a source for tropospheric nitrous acid. Nature Geosci. 4, 440–443.

595 Table 1. HONO source and sink mechanisms considered for modeling HONO in the outflow of the DFW metropolitan area.

Mechanism	ID	Parameter	Lower-limit	Likely	Upper-limit	Reference
Aerosol uptake of NO_2	B1	γ_{NO2} (-)	2.0×10^{-7}	1.0×10^{-6}	5.0×10^{-6}	Kleffmann et al. (1998); Aumont et al.(2003)
Photoenhanced aerosol uptake of NO_2	B2	$\gamma_{NO2,hv}$ (-)	4.0×10^{-6}	1.0×10^{-5}	1.0×10^{-3}	Stemmler et al. (2007); Wong et al. (2013)
Photoenhanced conversion of NO_2 soot	B3	$\gamma_{soot,BET}$ (-)	4.0×10^{-7}	5.0×10^{-7}	6.0×10^{-7}	Monge et al. (2010)
		BET surface area (cm^2/g)	9.7×10^{5}	1.2×10^{6}	1.3×10^{6}	
Direct HONO emission	B4	f_{emiss} (%v, $\Delta HONO/\Delta NO_x$)	0.0029	0.0055	0.0080	Kirchstetter et al. (1996); Kurtenbach et al. (2001)
OH + NO	B5	$k\infty$(T) (cm^3 $molec^{-1}$ s^{-1})	3.0×10^{-11}	3.6×10^{-11}	4.3×10^{-11}	NASA (2011)
		k_o(T) (cm^6 $molec^{-2}$ s^{-1})	5.8×10^{-31}	7.0×10^{-31}	8.4×10^{-31}	NASA (2011)
HONO from surface HNO_3 photolysis	B6	$j_{HNO3\text{-}HONO}$ (s^{-1})	1.0×10^{-5}	1.2×10^{-5}	1.4×10^{-5}	Zhou et al. (2003)
		$v_{d,\ HNO3}$ (cm s^{-1})	1.50	1.75	2.25	Walcek et al. (1986)
HONO from NO_2 conversion at ground	B7	$\gamma_{NO2,\ gr}$ (-)	1.0×10^{-6}	5.0×10^{-6}	1.0×10^{-5}	Kleffmann et al. (1998); Kurtenbach et al. (2001)
Photoenhanced NO_2 conversion, ground	B8	$\gamma_{NO2,gr,hv}$ (-)	1.7×10^{-5}	2.0×10^{-5}	6.0×10^{-5}	Stemmler et al. (2006); Wong et al. (2013)
HNO_3 →HONO, VOC	S1	$f_{HNO3,\ VOC}$ (ppt s^{-1})	3.6×10^{-2}	5.8×10^{-2}	8.3×10^{-2}	Rutter et al. (2014)
Biotic release, ground	S2	f_{soil} (molec cm^{-2} s^{-1})	-	1.7×10^{9}	4.0×10^{9}	Oswald et al. (2013)
Re-emission from NO_2-(p) reservoir	S3	$v_d \times \eta$ (cm s^{-1})	1.0×10^{-2}	9.0×10^{-2}	2.0×10^{-1}	Vandenboer et al. (2014)
HONO uptake at ground	L1	$\gamma_{HONO,gr}$ (-)	1.0×10^{-4}	2.0×10^{-5}	1.8×10^{-5}	Vandenboer et al. (2013); Wong et al. (2013); Trick (2004)
HONO + OH	L2	$k_{HONO+OH}$ (cm^3 $molec^{-1}$ s^{-1})	6.75×10^{-12}	4.5×10^{-12}	3.0×10^{-12}	NASA (2011)
HONO photolysis	L3	j_{HONO} (s^{-1})	1.8×10^{-3} - 3.9×10^{-5} [a]			This investigation

596 [a]Maximum-minimum range of the experimentally determined time-series values of j_{HONO} input to the model (not varied).

Table 2. Best estimates of parameterizations of sources and sinks of HONO in the outflow of DFW for baseline and scenario GrN S2/S3.

		Best-fit estimate (% difference from 'likely')	
ID	**Parameter**	**GrN S2, S3**	**GrN Baseline**
B1	γ_{NO2} (-)	3.9×10^{-6} (294%)	2.5×10^{-6} (152%)
B2	$\gamma_{NO2,hv}$ (-)	8.5×10^{-4} (8500%)	1.0×10^{-3} (9900%)
B3	$\gamma_{soot,BET}$ (-)	5.3×10^{-7} (6%)	5.3×10^{-7} (7.1%)
	BET surface area (cm^2/g)	1.1×10^{2} (-6.5%)	1.2×10^{2} (-3%)
B4	f_{emiss} (%v, $\Delta HONO/\Delta NO_2$)	0.0043 (-22%)	0.0049 (-10%)
B5	$k\infty$(T) (cm^3 $molec^{-1}$ s^{-1})	3.7×10^{-11} (4.4%)	3.8×10^{-11} (4.8%)
	k_o(T) (cm^6 $molec^{-2}$ s^{-1})	7.6×10^{-31} (9%)	7.3×10^{-31} (4.8%)
B6	$j_{HNO3\text{-}HONO}$ (s^{-1})	1.2×10^{-5} (-3%)	1.3×10^{-5} (7.7%)
	$v_{d,\ HNO3}$ (cm s^{-1})	1.8 (4.6%)	2.0 (17%)
B7	$\gamma_{NO2,\ gr}$ (-)	6.1×10^{-6} (22%)	9.9×10^{-6} (97%)
B8	$\gamma_{NO2,gr,hv}$ (-)	6×10^{-5} (200%)	6×10^{-5} (200%)
S1	$f_{HNO3,\ VOC}$ (ppt s^{-1})	n/a	n/a
S2	f_{soil} (molec cm^{-2} s^{-1})	2.8×10^{9} (66%)	n/a
S3	$v_d \times \eta$ (cm s^{-1})	0.18 (105%)	n/a
L1	$\gamma_{HONO,gr}$ (-)	5.7×10^{-5} (185%)	2.0×10^{-5} (-1.1%)
L2	$k_{HONO+OH}$ (cm^3 $molec^{-1}$ s^{-1})	5.7×10^{-12} (28%)	4.6×10^{-12} (2.1%)
L3	j_{HONO} (s^{-1})	unchanged	unchanged
	Missing source or sink: daytime, nighttime (ppt s^{-1})	0.10, -0.0112	0.15, -0.006

Figure1

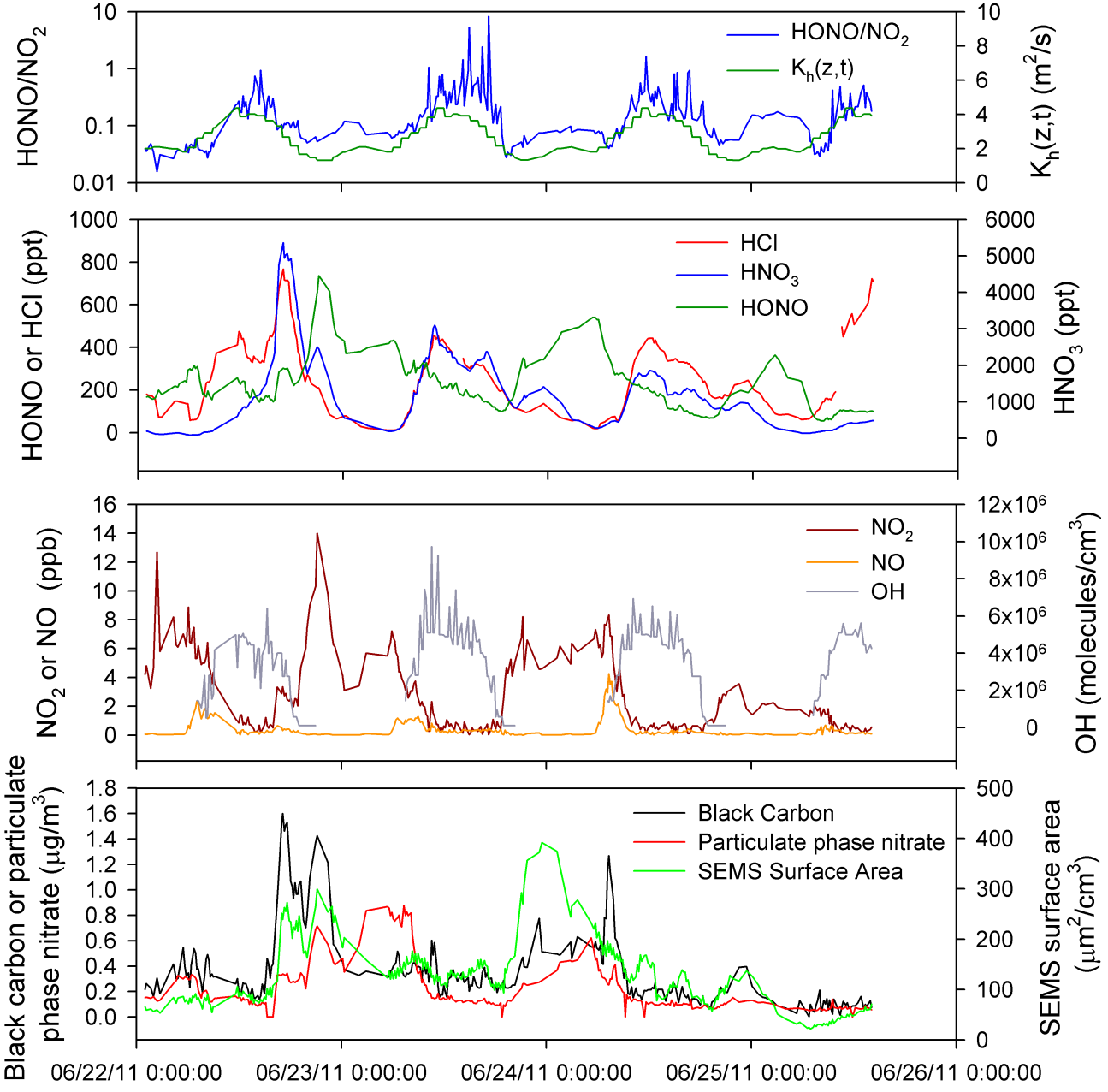

Figure 1. Time series inputs to the two-layer box model of HONO mixing ratios in the outflow of DFW.

Figure2

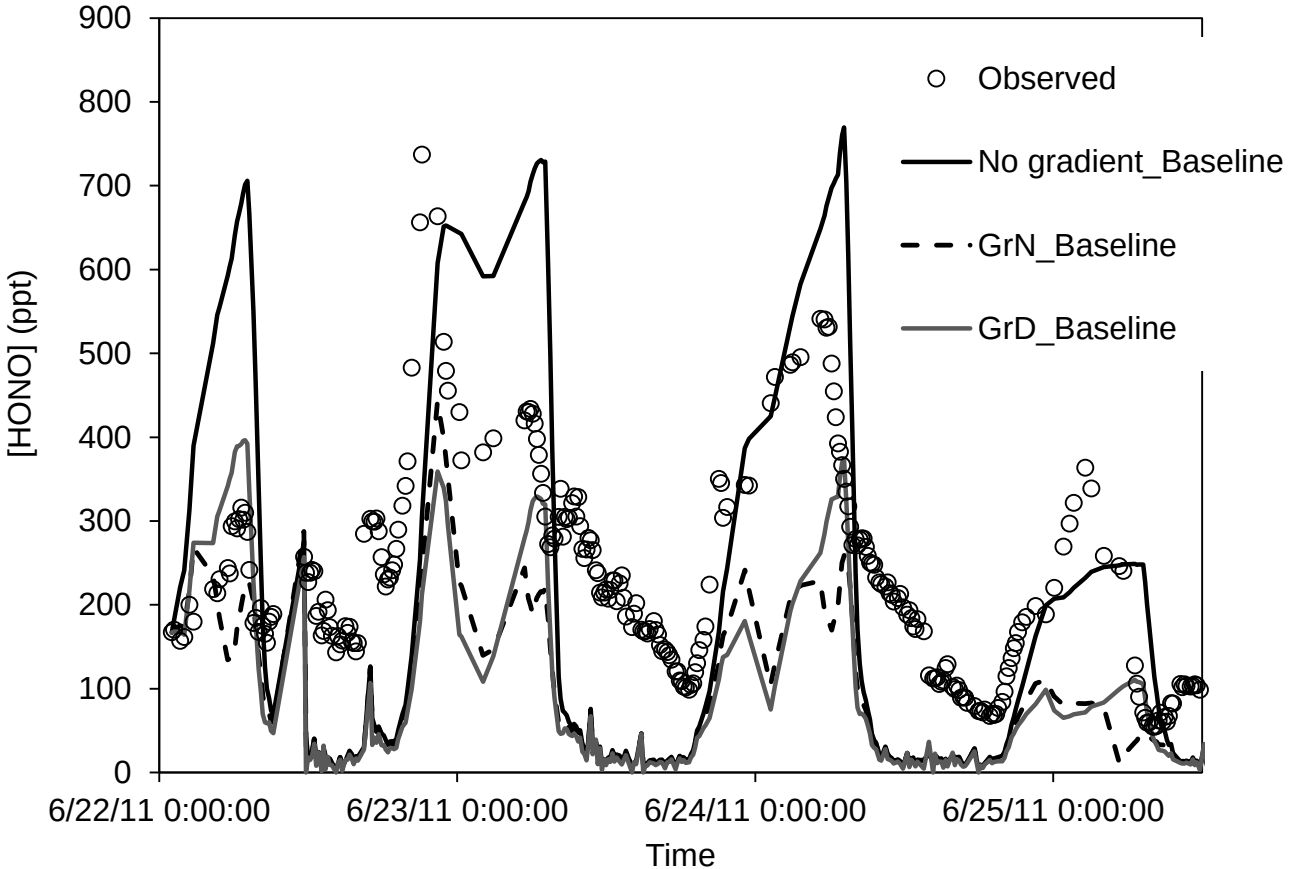

Figure 2. Model output for 'likely' estimates of parameterizations under conditions of no gradient, stronger nighttime gradient (GrN), and stronger daytime gradient (GrD).

Figure3

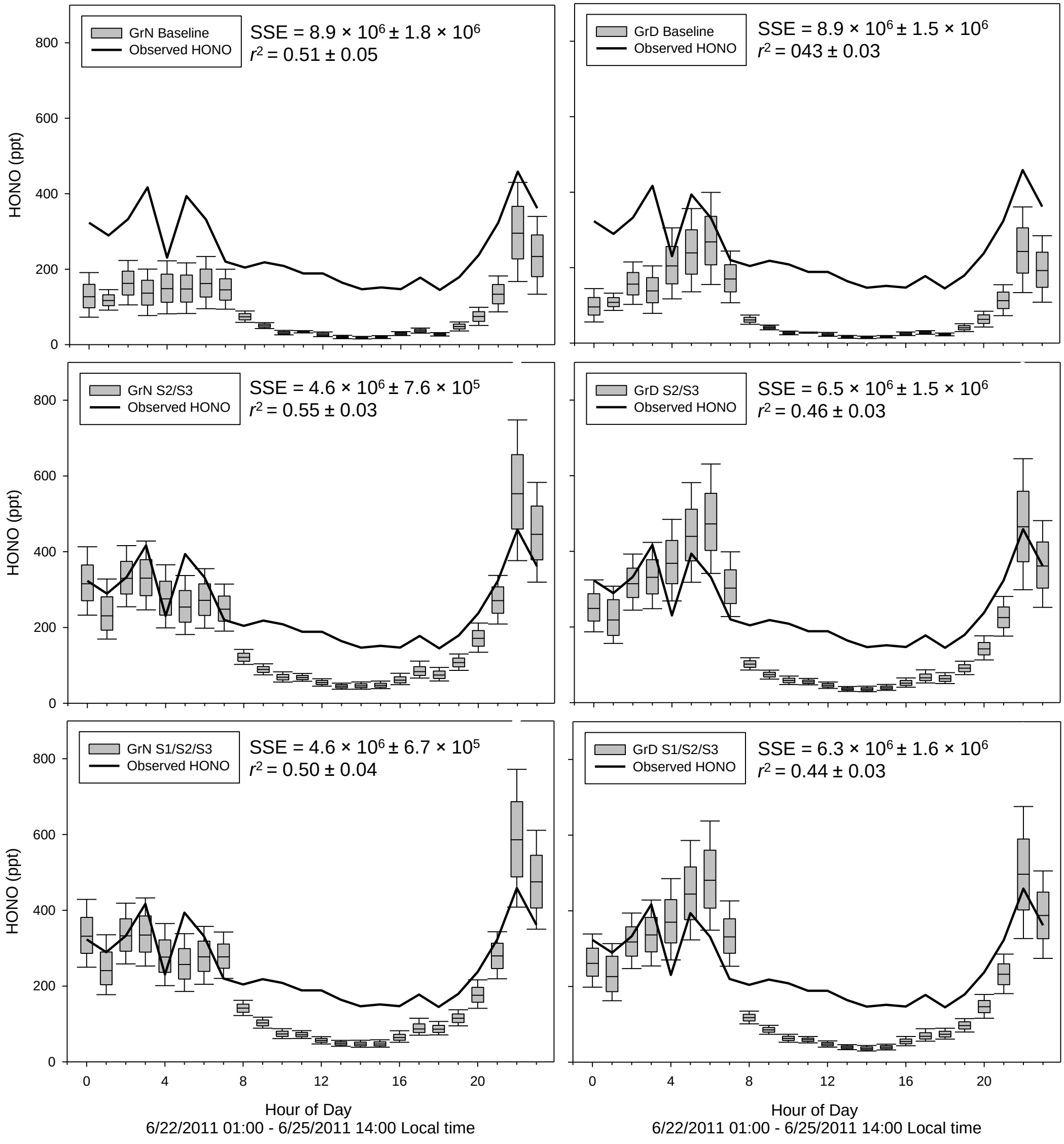

Figure 3. Summary of Monte Carlo simulation output for baseline scenarios, and scenarios with S2/S3 and S1/S2/S3 added to the baseline scenario.

Figure4

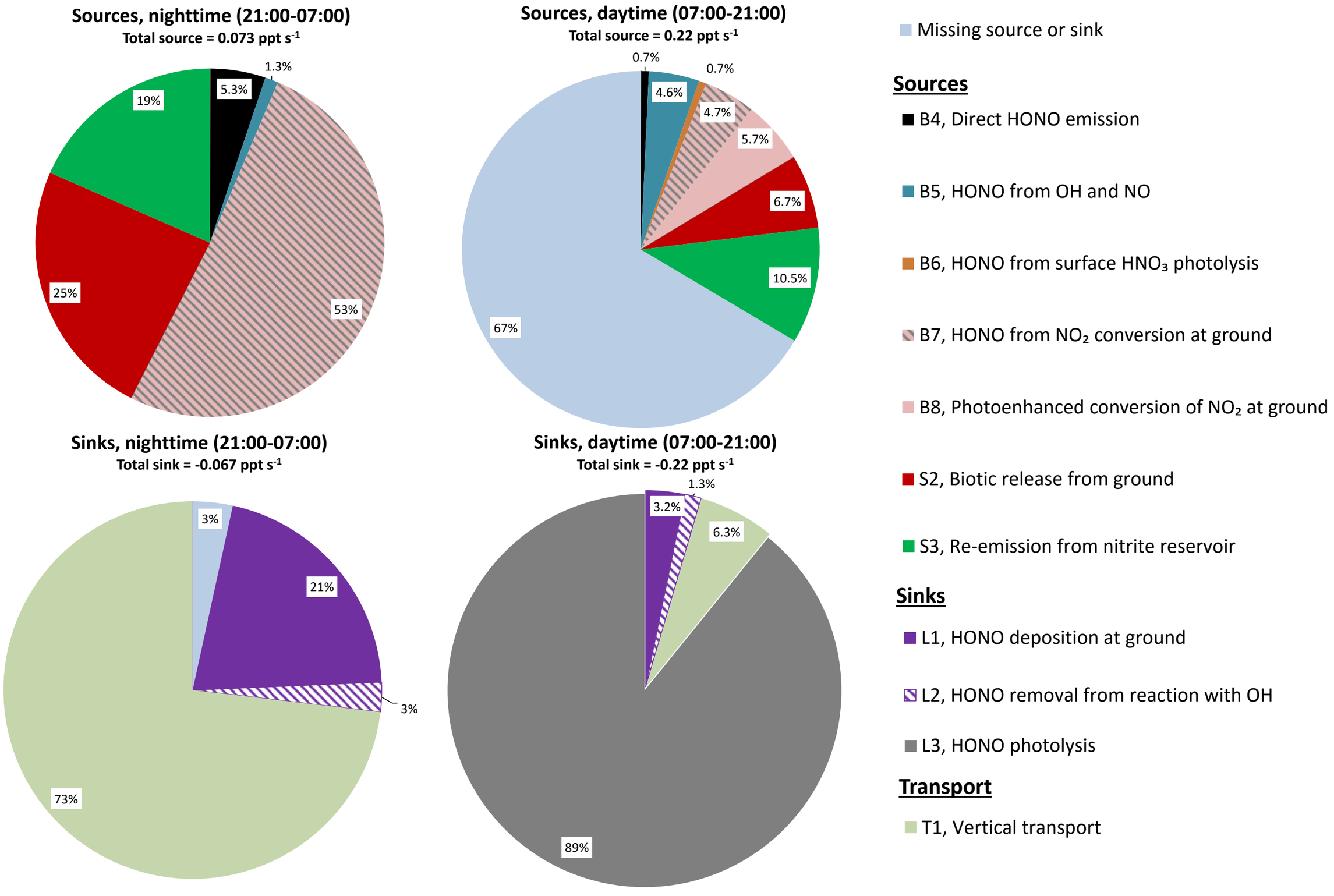

Figure 4. Relative contribution to HONO source or sink strength in GrN S2/S3 with 'likely' estimates of parameterizations. Contributions are averaged for the time period indicated above each pie chart across the modeling period (6/22/2011 01:00 – 6/25/2011 14:00 local time). Unknown source or sink is determined by stepwise addition of HONO source or sink such that modeled HONO equals measured HONO.

Figure5

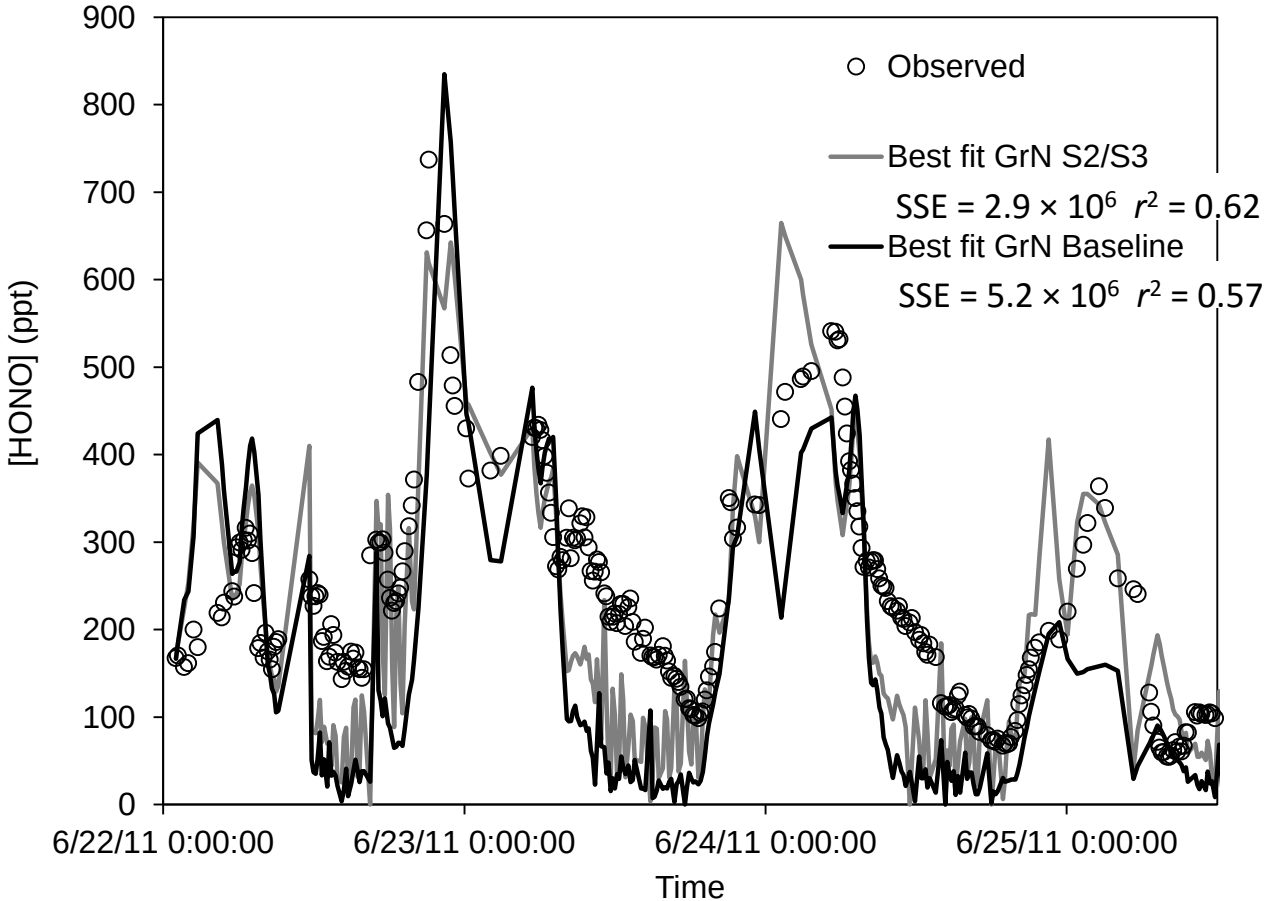

Figure 5. Model performance with best-fit parameters for the nighttime gradient (GrN) scenario with sources S2 and S3, compared to the nighttime gradient scenario with only baseline sources included.

Supplementary Material

Click here to download Supplementary Material: Gall et al_SI_rev10.docx